

University of Plymouth

PEARL

<https://pearl.plymouth.ac.uk>

01 University of Plymouth Research Outputs

University of Plymouth Research Outputs

2016-11-01

"This is an accepted manuscript of an article published by Elsevier in *Lithos* 2016 available at: <http://dx.doi.org/10.1016/j.lithos.2016.08.024>"

Please cite this article as: Coggon, R.M., Teagle, D.A.H., Harris, M., Davidson, G.J., Alt, J.C. & Brewer, T.S. (2016) Hydrothermal contributions to global biogeochemical cycles: Insights from the Macquarie Island ophiolite. *Lithos* 264, 329-347

**Hydrothermal contributions to global biogeochemical cycles:
Insights from the Macquarie Island ophiolite**

Submitted to Lithos

Rosalind M. Coggon^{a*} *R.M.Coggon@southampton.ac.uk*
Damon A.H. Teagle^a *Damon.Teagle@southampton.ac.uk*
Michelle Harris^{a,b} *michelle.harris@plymouth.ac.uk*
Garry J. Davidson^c *Garry.Davidson@utas.edu.au*
Jeffrey C. Alt^d *jalt@umich.edu*
Timothy S. Brewer^e

a. Ocean and Earth Science, National Oceanography Centre Southampton, University of
Southampton, European Way, Southampton, SO14 3ZH, UK.

b. School of Geography, Earth and Environmental Sciences, Plymouth University,
Plymouth, PL4 8AA, UK.

c. ARC Centre for Excellence in Ore Deposit Research (CODES), School of Physical
Sciences, University of Tasmania, Private Bag 79, Hobart, Australia 7001.

d. Earth and Environmental Sciences, University of Michigan, 2534 C.C. Little
Building, 1100 North University Ave, Ann Arbor, MI 48109-1005, USA.

e. Department of Geology, University of Leicester, University Road, Leicester, LE1
7RH, UK (deceased).

* Corresponding author

25

26 **Highlights:**

- 27 • Macquarie Island comprises a unique complete section of altered ocean crust.
- 28 • The Macquarie crust was a net source of Si, Ti, Al, and Ca to the oceans.
- 29 • The Macquarie crust was a net sink for H₂O, Mg, Na, K, and S.
- 30 • Veins make important contributions to hydrothermal chemical exchange budgets.

31

32

Abstract

Hydrothermal circulation is a fundamental process in the formation and aging of the ocean crust, with the resultant chemical exchange between the crust and oceans comprising a key component of global biogeochemical cycles. Sections of hydrothermally altered ocean crust provide time-integrated records of this chemical exchange. Unfortunately, our knowledge of the nature and extent of hydrothermal exchange is limited by the absence of complete oceanic crustal sections from either submarine exposures or drill core. Sub-Antarctic Macquarie Island comprises ~10 Ma ocean crust formed at a slow spreading ridge, and is the only sub-aerial exposure of a complete section of ocean crust in the ocean basin in which it formed. Hydrothermally altered rocks from Macquarie Island therefore provide a unique opportunity to evaluate the chemical changes due to fluid-rock exchange through a complete section of ocean crust. Here we exploit the immobile behavior of some elements during hydrothermal alteration to determine the precursor compositions to altered Macquarie whole rock samples, and evaluate the changes in bulk rock chemistry due to fluid-rock interaction throughout the Macquarie crust. The extent to which elements are enriched or depleted in each sample depends upon the secondary mineral assemblage developed, and hence the modal abundances of the primary minerals in the rocks and the alteration conditions, such as temperature, fluid composition, and water: rock ratios. Consequently the chemical changes vary with depth, most notably within the lava-dike transition zone where enrichments in K, S, Rb, Ba, and Zn are observed. Our results indicate that hydrothermal alteration of the Macquarie crust resulted in a net flux of Si, Ti, Al, and Ca to the oceans, whereas the crust was a net sink for H₂O, Mg, Na, K, and S. Our results also demonstrate the importance of including the contribution of elemental

uptake by veins for some elements (e.g., Si, Fe, Mg, S). Extrapolation of our results, assuming a crustal production rate of 3 km²/yr, yields estimates of the hydrothermal contribution to global geochemical cycles. For example, the Mg flux to the crust is estimated to be $3.3 \pm 1.1 \times 10^{12}$ mol/yr, sufficient to balance the riverine Mg input to the oceans given the uncertainties involved. However, the relationship between spreading rate and hydrothermal chemical exchange fluxes remains poorly understood, and the approach described here should be applied to crust produced at a range of spreading rates to refine the global hydrothermal flux estimates.

Keywords:

Ocean crust, hydrothermal alteration, biogeochemical cycles, Macquarie Island, ophiolite.

Abbreviations:

LDTZ = lava-dike transition zone; DGTZ = dike-gabbro transition zone; Mg# = $100 \times \text{Mg}/[\text{Mg} + \text{Fe}^{2+}]$, calculated assuming that 90% of the total iron is Fe²⁺; LOI = loss on ignition; MORB = mid-ocean ridge basalt.

1. Introduction

Hydrothermal circulation is an important component of global biogeochemical cycles. Chemical exchange between seawater and the ocean crust influences the composition of the oceans, the ocean crust, and via subduction the composition and heterogeneity of the mantle. Despite nearly 50 years of scientific ocean drilling, the ultimate goal of drilling a continuous in situ section through the entire ocean crust has not yet been achieved (Teagle and Ildefonse, 2011). The absence of complete oceanic crustal sections makes full quantification of the ocean crust's primary compositions and its hydrothermal contributions to global geochemical cycles difficult. In particular, our knowledge of the nature and extent of fluid-rock interaction in the lower crust is limited by the absence of accessible submarine exposures or drill core. Ophiolites, sub-aerially exposed sections of crust formed via seafloor spreading and subsequently emplaced on continental margins, have been used to investigate chemical exchange between seawater and the ocean crust (e.g., Bednarz and Schmincke, 1989; Gregory and Taylor, 1981). However, most intact ophiolites formed in supra-subduction settings and whether these outcrops are representative of normal mid-ocean ridge crust remains controversial (Miyashiro, 1973; Rautenschlein et al., 1985). These ophiolites are more intensely recrystallized, and consistently record a greater extent of fluid-rock exchange than crust from mid-ocean ridges (Alt and Teagle, 2000; Bickle and Teagle, 1992).

Sub-Antarctic Macquarie Island is the only sub-aerial exposure of a complete section of ocean crust in the open-ocean basin in which it formed (Varne et al., 2000; Varne et al., 1969). Macquarie Island provides a unique opportunity to investigate how the ocean

crust is accreted, including the role of hydrothermal circulation in cooling the upper and lower crust and the resultant fluid-rock chemical exchange.

Chemical exchange between hydrothermal fluids and the crust is facilitated by mineral dissolution and the formation of secondary minerals, which replace igneous minerals and mesostasis, fill primary porosity (vugs and interstices) and form veins. Hydrothermally altered rocks therefore provide a time-integrated record of the effects of fluid-rock exchange on the composition of the crust. Here we evaluate the hydrothermal changes in bulk rock chemistry of Macquarie Island rocks, and compare our results with other independent estimates of seawater-ocean crust hydrothermal exchange.

2. Macquarie Island

Sub-Antarctic Macquarie Island (54°30'S, 158°56'E) in the Southern Ocean comprises ~10 Ma ocean crust formed during slow spreading (10 mm/yr half rate) along the Australian-Pacific plate boundary (Armstrong et al., 2004; Duncan and Varne, 1988; Quilty et al., 2008; Varne et al., 2000). Spreading initiated along this boundary during the Eocene when the Tasman Sea rifted from the Campbell Plateau along a series of short ridge segments separated by fracture zones (Sutherland, 1995). Subsequent migration of the pole of Australian-Pacific relative plate motion caused progressive re-orientation of the spreading segments, producing the distinctive regional fracture zone curvature, with the system ultimately entering a dextral transpressional regime when extension was sub-parallel to the plate boundary (Cande et al., 2000; Lamarche et al., 1997; Massell et al., 2000; Sutherland, 1995). Shortening along the boundary uplifted the Macquarie Ridge Complex, exposed at Macquarie Island since ~0.6 Ma (Adamson

et al., 1996). The island comprises crust formed as the magmatism waned, with rocks from all crustal levels and the uppermost mantle exposed (Fig. 1) (Varne et al., 2000; Wertz et al., 2003).

Basaltic lavas crop out across the southern three quarters of the island and on North Head (Fig. 1). To the northwest is an uplifted section of intrusive ocean crust comprising a sheeted dike complex, massive gabbros, layered gabbros, and a cumulate sequence of ultramafic rocks (Fig. 1), with the underlying residual mantle harzburgites exposed at Eagle Point. The extrusive portion of this block is not exposed, but a sequence of steeply dipping sheeted dikes that grade upwards into gently dipping lavas occurs within a 5 km wide fault-bounded block on the west coast near Double Point and Mount Waite, within which the original seafloor relationships are preserved and the lava-dike boundary is the original extrusive-intrusive crustal transition zone (Davidson et al., 2004).

Three major faults juxtapose rocks from different crustal levels or metamorphic grade (Selkirk et al., 1990; Varne et al., 2000) (Fig. 1). The Finch-Langdon Fault separates the intrusive crustal section from lavas to the south. It is cemented by hydrothermal minerals, has talus breccias with clasts of basalt, dolerite and gabbro and is overlain by lava flows, consistent with it being a relict axial seafloor spreading fault (Wertz et al., 2003). The Isthmus fault emplaces greenschist facies dikes against the lower grade North Head lavas and the Major Lake Fault Zone emplaces sheeted dikes and lavas against extrusives of a lower metamorphic grade (Daczko et al., 2005; Lewis, 2007;

Portner et al., 2010; Rivizzigno and Karson, 2004). There are numerous other minor faults throughout the island (Goscombe and Everard, 2001).

All levels of the Macquarie crust have been affected by fluid-rock interaction. O and C isotopic analyses reveal that the crust interacted with seawater-derived fluids, rather than meteoric water. The lavas interacted with cold seawater at high water: rock ratios, whereas the lower crust interacted with hotter (300-600 °C) hydrothermal fluids at low water: rock ratios (Cocker et al., 1982).

2.1 Macquarie Island sample transects and stratigraphic reconstruction

Using the published geological maps (Goscombe and Everard, 1998a), supplemented by our own field observations, we selected three transects through the Macquarie crust to develop a complete ocean crustal section: a parallel pair of transects through the upper crust near Mount Waite and Double Point (A and B, Fig. 1); and the coastal Isthmus to Eagle Point transect through the intrusive crust and uppermost mantle (C, Fig. 1).

2.1.1 Mount Waite and Double Point transects

The Mount Waite transect traverses a narrow (<50 m) zone of steeply dipping (~75° W) sheeted dikes and the overlying extrusive rocks (Fig. 2a). The extrusive sequence consists of variably (<5 % to >30 %) plagioclase-phyric pillow lavas, volcanoclastic breccias and turbiditic sediments, dipping 20 - 30° E. Pillow units are typically 50-100 m thick, and can be traced laterally for several kilometers. The lavas are pervasively altered. The upper lavas contain smectite, iron-oxides and carbonate, typical of low temperature 'ocean floor weathering' (Alt et al., 1986), whereas the underlying lavas

were partially altered under zeolite or lower greenschist facies conditions and contain chlorite \pm zeolites \pm smectite \pm calcite \pm albite \pm prehnite \pm epidote. The inter-lava sediments include 1-10 m thick graded conglomerate, sandstone and red shale beds. Assuming the paleo-vertical is perpendicular to the lava flows, the extrusive section is ~850 m thick. A small volcanic cone of radially outward dipping elongate pillow lavas near Pyramid Peak, to the east of Mount Waite, indicates that the top of the Mount Waite extrusive sequence was at or near the paleo- seafloor (Griffin and Varne, 1980). The lava-dike transition (LDTZ) is therefore reconstructed to 850 m below seafloor, with sample depths assigned from this datum.

The Double Point transect is similar to the Mount Waite transect, but with a greater expanse of sheeted dikes exposed (Fig. 2b). The dikes are 1.5 to 3 m wide, with narrower cross-cutting dikes increasingly abundant up section (Davidson et al., 2004), and are partially altered under greenschist facies conditions (Table S1). The LDTZ is cut by minor faults with disseminated pyrite and chlorite halos (Davidson et al., 2004). Similar sulfide anomalies have been identified at the LDTZ in ocean crust from ODP Holes 504B and 1256D, and the Troodos ophiolite, Cyprus (Alt, 1994, 1995b; Alt et al., 2010). A 40 m wide fault zone with epidote-actinolite-zoisite-quartz-chalcopryrite-pyrite veins is interpreted as a hydrothermal upwelling site (Davidson et al., 2004). The lavas at the western tip of Double Point were altered under greenschist to amphibolite facies conditions and were intruded by the dikes during spreading (Davidson et al., 2004), consequently the transect is treated as a continuous section. Sample depths are assigned assuming the paleo-vertical is perpendicular to the bedding, and the LDTZ was 850 m below seafloor.

2.1.2 The Isthmus-Eagle Point transect

Sheeted dikes are exposed in Hasselborough Bay. The dikes are typically 0.5-3 m wide and can be traced laterally <30 m along strike. They are sub-parallel, and their chilled margins dip ~60° SW on average (Fig. 3). Some dikes enclose and are chilled against gabbro screens that make up <5% of the outcrops. The dikes are aphyric to highly plagioclase phyric, with increasing phenocryst abundance and grain size of groundmass and phenocrysts away from the well-defined chilled margins. Both porphyritic and aphyric dikes occur throughout the sheeted dike section, cross-cut by later stage narrow (~10 cm wide) aphyric dikes. The dike-gabbro transition (DGTZ) is characterized by an increase in size and abundance of gabbro screens and a decrease in the abundance of dolerite dikes. The sheeted dikes were altered under greenschist facies conditions, with amphibolite grade dikes in the DGTZ. The most intense alteration typically occurs in 'halos' that flank veins.

The lower crust is predominantly massive gabbro with enclaves of anorthosite and olivine gabbro. Compositional layering is restricted to Handspike Point where felsic and mafic layering is oriented ~126/48°SW, sub-parallel to sheeted dike margins indicating it was originally sub-vertical. The gabbros are typically fresher than the overlying sheeted dikes and were altered under greenschist to amphibolite facies conditions (Table S1). The alteration is highly heterogeneous and most intense adjacent to veins. Sub-parallel amphibole + chlorite veinlets impart a weak fabric and are cut by wider (<5 mm) epidote + prehnite veins and later-stage cataclastic prehnite + chlorite veins. Dolerite dikes similar to those of the sheeted dike complex occur throughout the gabbro,

but were altered under similar conditions to the host gabbro. Narrower (<40 cm) microgabbro dikes and veins are common, with diffuse margins suggesting emplacement before the host gabbro had completely cooled. The transition between the gabbro and the underlying harzburgite comprises a complex association of highly to completely altered ultramafic rocks including dunite, plagioclase dunite, wehrlite, plagioclase wehrlite, olivine gabbro, troctolite and harzburgite. The contacts between the rock units are poorly constrained by limited exposure. Troctolite exposed at Elizabeth and Mary Point contains alternating mafic and felsic layers that dip ~30° east-northeast. The layers are sub-parallel and typically a few centimeters to tens of centimeters thick. Increasing plagioclase abundance upwards within layers indicates they are the correct way up (Goscombe and Everard, 2001). Dolerite sills intrude the troctolite at an oblique angle to the layering. The harzburgite exposed at Eagle Point is massive, serpentinized, and intruded by pegmatitic gabbro and rare <1 m wide plagioclase phyric dolerite dikes that are pervasively prehnitized or rodingitized. The paleo-vertical of this section is constrained to lie within the average plane of the dolerite dike chilled margins, which dips ~ 60° SW. The troctolite compositional layering is orthogonal to the sheeted dikes' chilled margins, with the pseudo sedimentary structures indicating they are paleo-horizontal layers. Its pole is therefore taken as the paleo-vertical for this transect (Fig. 3b).

2.2 The proto-Macquarie Island ocean crust

Although slow-spread ocean crust is architecturally complex (e.g., Cannat et al., 2008; MacLeod et al., 2009), layered crust similar to that formed at fast spreading rates (Penrose Conference Participants, 1972) may be produced at the middle of relatively

robust slow-spreading accretionary segments (Dick et al., 2003; Dick et al., 2006; Sinha et al., 1998). The proto-Macquarie Island crust includes all the components of normal layered ocean crust. Our sample transects are combined to give a complete section through this crust, with the LDTZ of the Mount Waite and Double Point transects aligned at 850 meters below seafloor (mbsf), and the alteration assemblages of the sheeted dikes of the Eagle Point-Isthmus and Double Point transects correlated (Fig. 4). Our composite section is similar to previous Macquarie stratigraphies (Dijkstra and Cawood, 2004; Goscombe and Everard, 1998b), but with significantly different layer thicknesses. This in part reflects considerable lateral variability in crustal layer thicknesses across Macquarie Island, for example the maximum exposed thickness of lavas is 1.4 km. Goscombe and Everard (1998b) use the average thickness of gabbro in other ophiolites, which is approximately double the maximum gabbro thickness observed on Macquarie Island. The reconstructed thickness of the proto-Macquarie crust (3-4 km; Fig. 4) is consistent with its formation on a short segment of a slow spreading ridge in a waning magmatic system (Cannat, 1996; Chen, 1992; Dick et al., 2003).

The syn-volcanic tectonism along the Finch-Langdon Fault (Rivizzigno and Karson, 2004; Wertz et al., 2003) and the intrusion of dolerite dikes into relatively cool gabbros and harzburgite indicate that the Macquarie crust was generated during multiple magmatic episodes alternating with periods of tectonic extension, analogous to the ‘tectono-magmatic cycles’ observed at slow-spreading ridges (Sinha et al., 1998). The timing of the different magmatic events remains poorly constrained, and the co-genetic relationships between the different units unknown. For example, the majority of

Macquarie basalts have highly enriched mid-ocean ridge basalt (MORB) compositions indicative of small-degrees of fractional melting (Kamenetsky et al., 2000) that are not consistent with their formation during the melting event that depleted the Macquarie upper mantle (Wertz, 2003). Despite its formation during multiple magmatic events, Macquarie Island represents the best available continuous section through the lower ocean crust produced at a slow-spreading ridge and complements lower crustal sections drilled at slow spreading ridges into gabbro (for example ODP Hole 735B and IODP Hole 1309D; (Blackman et al., 2006; Dick et al., 1999; Robinson et al., 1989)).

3. Analytical Techniques

Representative samples (> 1 kg) were taken every 20 m along transects orthogonal to bedding at Double Point and Mount Waite, with additional samples taken from fracture zones. Along the steep cliff sections of these transects the outcrop is nearly continuous, with soft sediment interbeds preserved in the walls of transecting gullies. Along the Isthmus – Eagle Point coastal transect outcrops are discontinuous, separated by cobble beaches and areas of marshland. Large samples (1-5 kg) representative of the rock types in each outcrop were taken.

Thin sections were prepared to include the variations in igneous, metamorphic, or tectonic features. Samples for whole rock geochemical analyses were cut, using a diamond saw, avoiding these heterogeneities with sub-samples of more intensely altered zones prepared for comparison. Exterior weathered surfaces were removed, and samples were ultrasonicated in deionized water, dried for 12 hours at 70°C, fragmented to <1 cm chips between sheets of clean paper in a hardened pure-iron fly press, and powdered

using a hardened pure-iron tema. Lithologies were determined from the modal mineralogy. The key petrographic features of each rock type are summarized in Table S1.

Geochemical analyses of 236 Macquarie Island whole rock samples are presented in Table S2. Major and trace elements were analyzed by X-ray fluorescence (XRF), following the methods of Brewer et al., (1998), using a PW1400 X-Ray Spectrometer at the University of Leicester. Geochemical reference materials were used to construct calibrations for individual elements and to evaluate precision and accuracy (Table S3). A subset of samples were analyzed at the University of Tasmania School of Earth Sciences using a PW1410XRF, following the methods of Norrish and Hutton (1969). Carbon and Sulfur concentrations were analyzed using a LECO Carbon/Sulfur Analyser by high-temperature combustion, at the University of Leicester. The lower limit of detection was 10 ppm, with a precision of $\pm 5\%$ and $\pm 8\%$ for C and S, respectively.

Trace elements concentrations were determined by Inductively Coupled Plasma Mass spectrometry (ICP-MS) at the University of Southampton using a VG PlasmaQuad PQ2+. Precision and accuracy were better than $\pm 5\%$ RSD and $\pm 8\%$ RMSD, respectively, for the majority of elements (Table S4).

4. Primary magmatic diversity of Macquarie Island igneous rocks

Published analyses of fresh glasses from Macquarie Island hyaloclastites and pillow margins reveal they are basaltic in composition, with 47.4-51.1 wt% SiO₂ and 5.65-8.75 wt % MgO, but range from depleted N-MORB to compositions more enriched than

typical E-MORB (Kamenetsky et al., 2000; Wertz, 2003). They span a wider range in K_2O content (0.1-0.8 wt%) than usual for a single MORB suite (Kamenetsky et al., 2000) and span most of the range in Zr/Y ratios of other MORB suites combined (Fig. 5a). This diversity reflects a complex melting history. Glass compositions have been divided into two groups on the basis of their Mg-numbers ($Mg\# = 100 \times Mg/[Mg + Fe^{2+}]$) and K_2O contents, Group 1 being those with the highest Mg-number at a given K_2O content (Kamenetsky et al., 2000). Group 1 glasses, which have the lowest Y concentrations at a given Zr concentration, are interpreted to be near-primitive 'parental' melts from which Group 2 glasses fractionated (Kamenetsky et al., (2000); Fig. 5a). The seriate variation in parental melt compositions is attributed to an increasing degree of partial melting of a mantle source that is homogeneous on a large scale (Kamenetsky and Maas, 2002). This interpretation is supported by a progressive decrease in the degree of incompatible element enrichment up through several extrusive sequences on the island (Wertz, 2003). Aphyric lavas and dikes have Zr/Y ratios consistent with fractionation from parental melts with Group 1 glass compositions (Fig. 5b). The anorthosites and gabbros have similar Zr/Y ratios to the dikes and lavas produced by higher degrees of partial melting.

All whole rock samples are altered to some extent and alteration effects are superimposed on and may obscure primary magmatic compositional variations. However, there are variations in whole rock chemistry that correspond to changes in rock type, reflecting differences in primary mineral modal proportions, and hence are of magmatic origin. Consequently there are broad trends with depth; for example

decreasing concentrations of Ti, Fe, Na, P, K, Sr, Zr, and Nb and increasing Cr and Ca contents and magnesium number (Fig. 6).

Since Zr, Y, and the REEs are relatively immobile during hydrothermal alteration the Zr/Y and La/Sm ratios should record primary magmatic variations through the crust. In general the La/Sm ratio decreases with depth, despite significant variability at a given depth. Gabbros, dikes and lavas with similar Zr/Y and La/Sm ratios may be co-magmatic. Systematic variations in melt composition through the gabbro section due to cyclic magma chamber processes, such as fractionation and magma replenishment, cannot be distinguished given the sampling scale.

5. Calculating the chemical changes due to hydrothermal alteration

The impact of hydrothermal circulation on ocean chemistry depends on the changes in bulk rock chemistry due to seawater-rock interaction. As hydrothermal alteration of the ocean crust is pervasive the fresh igneous precursors to altered rocks are rarely preserved, and their compositions are difficult to determine if the altered rocks comprise a fractionated suite. However, the behavior of elements that remain immobile during hydrothermal alteration can be used to account for: (i) passive changes in elemental concentrations in response to net changes in mass; and (ii) the primary magmatic variation in precursor suites (Grant, 1982; Gresens, 1967; MacLean, 1990; MacLean and Barrett, 1993). During alteration, immobile element concentrations change only in passive response to net mass changes, being concentrated by bulk rock mass loss or diluted by mass gains (Fig. 7a). If one immobile element is incompatible (e.g. Zr, Y or Nb) and another is compatible, their fractionation trend is distinct to the alteration

trends, which radiate from the origin. Their concentrations in the precursor to a given altered rock can therefore be determined from the intersection of its alteration trend and the fractionation trend, established using fresh samples from the same fractionated suite (MacLean, 1990) (Fig. 7b). Similarly the precursor's mobile compatible element concentrations can be determined from their fractionation trends with the immobile incompatible element, also defined using the fresh samples, and the calculated precursor immobile incompatible monitor element concentration.

Determining fresh precursor compositions for Macquarie Island rocks is challenging given the complex melting history of the ophiolite. For each immobile element pair the variable degree of partial melting produced a series of primitive parental melt compositions from which fractional crystallization yielded a large array of potential fresh precursor compositions (Fig 7c-d). Consequently, precursor immobile element concentrations are difficult to determine, unless the net mass change due to alteration is known. There is a weak correlation between the samples' specific gravity and LOI (Table S2; $R^2 = 0.3$, $n = 128$) indicating a slight decrease in density associated with hydration during alteration, which equates to less than a 5% decrease in mass assuming constant volume. In the following calculations we therefore assume that there is no net mass change during alteration, i.e. $M^A/M^0 = 1$, where M^A and M^0 are the total masses of an altered rock and its fresh precursor, respectively, but allow for 5% uncertainty in this ratio.

We also assume that: (i) Zr, Y, and Nb were immobile during alteration, and can be used as 'monitors' of magmatic fractionation to estimate precursor mobile element

concentrations; and (ii) fresh glasses and the least altered whole rock samples are representative precursors for the altered rocks. The Macquarie samples include eight pairs, each cut from variably altered portions of the same protolith. The more altered portions have the same Zr/Y and Nb/Y ratios as their less altered counterparts (Fig. 8) indicating that Y, Zr, and Nb were immobile during alteration. The least altered whole rock samples were identified petrographically and from their LOI, with low LOI indicating minimal addition of hydrous secondary minerals. The assumption that they represent fresh precursor compositions despite their slight alteration may result in the underestimation of some hydrothermal chemical changes.

The methods used to determine precursor compositions for different sample types are summarized in Figure 9. The precursors to samples crystallized from fractionated magmas (aphyric lavas and dikes, and non-cumulate plutonic rocks) are determined from the magmatic fractionation trends of compatible elements (e.g., Ti, Fe, Mn, Mg, Ca, Na and K) against immobile incompatible ‘monitor’ elements (Zr and Nb) defined by Macquarie glasses supplemented with the least altered dike, anorthosite, and gabbro samples to extend the range of precursor compositions. The interplay of varying degree of partial melting and extent of subsequent fractional crystallization produced a diverse range in Macquarie magma compositions (Fig 7). However, for each compatible element the extent to which the partial melting and fractional crystallization trends diverge against the immobile monitor elements varies. We have exploited this effect, selecting the immobile monitor element (Nb or Zr) that best constrains the primary magmatic trend for each compatible element (Table S5). Several elements (Si, Al, S, Zn and Lu) show no significant variation with Zr or Nb, and the precursor concentrations

adopted for each rock type are the average concentrations of the glasses and least altered samples (Table S5). Phenocryst accumulation in phyric samples causes deviations from primary magmatic fractionation trends. To determine precursor compositions for such rocks we must account for: (i) the types, abundances and primary compositions of phenocrysts; and (ii) primary magmatic variation of the groundmass. The former could be achieved by comparing samples to the least altered samples with similar phenocrysts abundances, but this does not compensate for primary variation in groundmass composition. Here, we attempt to account for the variation in phyric sample precursor composition using the average compositions of the least altered samples of similar Nb content (Table S6). We make a first order estimate of the hydrothermal chemical changes to cumulate olivine gabbros through comparison with the average composition of the least altered cumulate olivine gabbro samples (Table S6). All troctolite, dunite and harzburgite samples are significantly altered, and do not represent precursor compositions. Consequently we have not calculated the chemical changes associated with alteration of these rocks.

The change in mass of component i during alteration (Δm_i) is the difference between the mass of component i before (m_i^o) and after (m_i^A) alteration:

$$\Delta m_i = m_i^A - m_i^o \quad (1)$$

Where $m_i^A = c_i^A M^A$ and $m_i^o = c_i^o M^o$ (M^A and M^o are the total masses of the altered rock and its precursor, respectively, and c_i^A and c_i^o are their concentrations of component i). The mass of the rock after alteration can be determined from the change in concentration of an immobile element, c_x

$$M^A = \frac{c_x^o}{c_x^A} M^o \quad (2)$$

So Equation 1 can be rewritten:

$$\Delta m_i = M^0 \left[\left(\frac{c_x^0}{c_x^A} \right) c_i^A - c_i^0 \right] \quad (3)$$

Here we present changes in mass of each element during hydrothermal alteration, calculated from the analyzed whole rock compositions and their estimated precursor compositions using Equation 3, for an arbitrary initial sample mass (M^0) of 100 g (Fig. 10) and assuming the net mass change is less than 5% (i.e. $c_x^0/c_x^A = 1 \pm 0.05$). The errors in the calculated values of Δm_i are propagated on a sample-by-sample basis (Fig. 10) to include (i) analytical uncertainty, (ii) the uncertainty in the net change in mass; and (iii) the uncertainty in estimated precursor compositions (see Supplementary Material).

6. Hydrothermal changes in Macquarie Island whole rock chemistry

In the following discussion depths (m) refer to the crustal depth within the proto Macquarie Island crust (Fig. 4). The calculated hydrothermal changes in whole rock chemistry (Δm_i) are presented as absolute values (per 100g of initial sample; Fig. 10), to enable comparison between lithologies and evaluation of hydrothermal exchanges within the crust. The crust is divided into 25-400 m thick intervals and the mean Δm_i within each interval are calculated assuming the samples are representative of the lithologies and their proportions in that interval. The results (termed ‘depth-averaged’ data) are presented in Figure 11. The thicknesses of the selected intervals reflect stratigraphic horizons in the section (e.g. the 25 m LDTZ) and the sampling frequency versus depth, with depth intervals containing 2-27 samples. The average relative changes in composition of each rock type are summarized in Table 1.

The most significant change in Macquarie Island whole rock chemistry is the increase in volatile content, which we have determined from altered samples' loss on ignition (LOI) and their estimated precursor H₂O contents. A sample's LOI gives an indication of its volatile content, offset by the increase in mass due to oxidation of ferrous iron during combustion. Provided the Fe²⁺/Fe³⁺ ratio is known and there was complete oxidation of the ferrous iron, this effect can be corrected for using $LOI_{actual} = LOI_{measured} + 0.11 \text{ FeO (wt\%)}$ (Lechler and Desilets, 1987). Assuming that 90% of the total iron is Fe²⁺ the average Fe contents of the Macquarie lavas, dikes and gabbros correspond to an additional LOI of 0.79, 0.82 and 0.41 wt% respectively. Consequently the hydrothermal increases in volatile content of Macquarie samples are likely underestimated here by ~0.4 – 0.8 g/100g. The increase in volatile content primarily reflects hydration and CO₂-uptake during fluid-rock interaction. Given limited sample material the C content was determined for only 55% of samples and LOI data are not corrected for CO₂ content. However, assuming that all C present in the analyzed samples occurs as CO₂, the CO₂ content of the majority of samples is less than 0.5 wt%, with CO₂ contents greater than 1 wt% only observed in five CaCO₃ bearing dike samples. The calculated increases in volatile content (up to 8.3g/100g) therefore primarily reflect the formation of hydrous secondary phases, including clay minerals, zeolites, chlorite, amphiboles, epidote, talc and serpentine. On average all lithologies are moderately to highly enriched in volatiles, but the calculated enrichment is typically lower for porphyritic lava and dike samples compared to the aphyric samples (Table 1) because the least altered whole rock samples chosen to represent precursor compositions are themselves partially hydrated (LOI <2 wt %) relative to the fresh Macquarie glasses (0.25 – 1.49 wt% H₂O (Kamenetsky et al., 2000; Wertz, 2003)). Samples from throughout the Macquarie crust are hydrated, with

harzburgite-hosted dike and gabbro samples from the base of the section (3300 m) enriched in volatiles by 3.1 and 2.3 g/100g but CO₂ contents of <0.1 wt%, indicating that hydrous fluids penetrated through the entire crustal section and into the uppermost mantle (Fig. 10). The greatest average enrichment (~2.5 g/100g) occurs in the uppermost sheeted dikes, between 850 and 950 m, decreasing with depth through the sheeted dikes to ~0.4 g/100g at 1550 m (Fig. 11).

6.1 Major elements

The changes in mass of the major element oxides are variable both within and between lithologies reflecting differences in secondary mineral assemblages, variations in the extent of fluid-rock interactions, and the thermal structure of the crust. SiO₂ was variably enriched or depleted throughout the crust, with Δ SiO₂ within error of zero for many samples due to the uncertainty in precursor compositions (Fig. 10). SiO₂ is on average depleted through most of the crust, but enrichments occur in the lavas (500-600 m), LDTZ, uppermost dikes (825-1050 m), and the DGTZ (1550-1650 m), where SiO₂ enrichment is associated with secondary quartz formation.

Titanium is usually assumed to be immobile during hydrothermal processes (Bednarz and Schmincke, 1991; MacLean and Barrett, 1993; Teagle et al., 1996), consistent with many Macquarie whole rock samples recording enrichments or depletions in TiO₂ within error of zero change (Fig. 10). Depth-averaged changes in TiO₂ reveal that the upper 200m of gabbros gained on average ~0.2 g/100g TiO₂, but Ti was immobile through the rest of the lower crust (Fig. 11). Ti was also enriched within the upper-

sheeted dikes (between 950-1050 m), but depleted or immobile through the lavas and lower sheeted dikes (Fig. 11). Enrichments likely reflect secondary titanite formation.

Each Macquarie lithology includes samples that were enriched and samples that were depleted in Al_2O_3 , CaO and Na_2O due to hydrothermal alteration (Fig. 10). The depth-averaged data indicate that whole rock samples were on average depleted in CaO and Al_2O_3 and enriched in Na_2O or experienced changes in these elements within error of zero throughout the majority of the Macquarie crust (Fig. 11). Depletions in Al_2O_3 and CaO associated with Na_2O enrichments reflect the replacement of calcic plagioclase by secondary albite, although the loss of CaO due to albitisation is partially compensated by the uptake of Ca in calcium carbonate minerals and prehnite. The plagioclase-phyric lavas are depleted in Al and Ca and enriched in Na , but to a lesser extent than the aphyric lavas and dikes (Fig. 10). This may be because the large plagioclase phenocrysts are relatively fresh in the porphyritic samples, except where they are intersected by veins. Alternatively, this difference could be an artifact of using 'least altered' whole rock samples to define the precursor compositions of porphyritic samples.

Changes in K_2O are variable throughout the Macquarie section (Fig. 10), but K_2O is on average enriched in all rock types except the aphyric dikes (Table 1). K_2O enrichment of the lavas (~ 0.2 g/100g on average) reflects potassium uptake from seawater-derived fluids into secondary celadonite and zeolite (phillipsite). The greatest average K_2O enrichment (~ 0.5 g/100g) occurs at the LDTZ, with the extent of K_2O enrichment decreasing down through the sheeted dikes. The greatest average K_2O enrichment in the

lower crust (0.25 g/100g) occurs between 2100 and 2200 m due to K₂O enrichment of anorthosites, in which plagioclase has been seritized.

Magnesium, iron and manganese were variably enriched or depleted throughout the Macquarie crust due to hydrothermal exchange, with changes reflecting the development of saponite, celadonite, Fe-oxyhydroxide and chlorite in the upper crust, and chlorite, amphibole (actinolite, tremolite and hornblende), talc and serpentine in the lower crust. There are significant enrichments in MgO, FeO, and MnO in the gabbros and olivine gabbros at ~2300 m of up to ~15, 3.5 and 0.07 g/100g, respectively (Fig. 10). These calculated enrichments should be treated with caution as they may be artifacts of estimated precursor compositions that do not adequately account for the primary mineral modal variation of these samples. However, they are associated with hydration of up to 8.3 g/100g, consistent with significant fluid-rock interaction that resulted in the replacement of olivine by talc + amphibole + chlorite + clay ± serpentine. The depth-averaged Δ MgO data indicate that MgO was enriched or within error of zero change throughout the crustal section, with the exception of the uppermost lower crust, which lost on average ~0.9 g/100g MgO (Fig. 11). In contrast FeO was on average depleted or within error of zero change throughout, with the only significant enrichments (<1.2 g/100g) occurring between 950 and 1050 m and below 2200 m. Depth averaged Δ MnO reveal variable enrichments or depletions within error of zero change through much of the Macquarie crust. However, MnO is on average enriched in the lowermost lavas and upper sheeted dikes, with the extent of enrichment increasing with depth to ~0.05 g/100g at 1050 m, but depleted in the uppermost lower crust (Fig. 11).

Changes in the sulfur content are typically small (< 0.1 g/100g) through the Macquarie crustal section and dominated by S-enrichment at the LDTZ (< 3.2 g/100g) where secondary sulfides are most abundant (Davidson et al., 2004). Above the LDTZ, the majority of aphyric lavas have lost ~ 0.08 g/100g S, whereas porphyritic lavas show no change (Fig. 10). This difference likely reflects a very early stage of alteration resulting in S-depletion that is not observed when comparing to ‘least altered’ porphyritic precursors that also experienced S-depletion. The average changes in S content due to hydrothermal alteration may therefore be underestimated here by 0.04 to 0.08 g/100g, depending on the relative proportion of the lavas that are porphyritic in each depth interval (50 – 100%). Similarly, aphyric dikes show greater S-depletions compared to porphyritic dikes. The LDTZ and upper sheeted dikes are on average enriched in S by ~ 0.5 and 0.05 g/100g, respectively, whereas the lower sheeted dikes are on average depleted in S. This is consistent with leaching of sulfur from the lower sheeted dikes by high temperature hydrothermal fluids (Alt, 1994, 1995b). In contrast the lower crust is on average enriched in S (Fig. 11).

Phosphorous is variably enriched or depleted throughout the Macquarie crustal section (Fig. 10). On average the gabbros, olivine gabbros and anorthosites are enriched in P_2O_5 (Table 1), but their absolute calculated ΔP_2O_5 values are small (< 0.01 g/100g) and generally within error of no change (Fig. 10) given the uncertainty in precursor P_2O_5 concentrations.

6.2 Trace elements

The base metals Cu and Zn were highly mobile during alteration of the Macquarie Island crust (Fig. 10). Cu is accommodated in fresh rocks by primary sulfides that typically occur as ‘blebs’ in the groundmass (Doe, 1994). The estimated precursor Cu contents of the porphyritic lavas and dikes ($\sim 25 \pm 7$) is lower than that of the aphyric rocks ($\sim 100 \pm 20$ ppm), which may reflect the lower proportion of groundmass in porphyritic rocks. Alternatively it could be an artifact of using ‘least altered samples’ as precursors to these rocks if they were depleted in sulfur and consequently Cu during early hydrothermal alteration. Cu is on average moderately depleted in the aphyric lavas and dikes (Table 1). Cu-depletion of the aphyric rocks is less pronounced at the LDTZ (Fig. 10) coincident with the zone where secondary sulfides including chalcopyrite are most abundant, indicating that the depletion is partially compensated by secondary mineralization. Aphyric dikes from the sheeted dike complex experienced a greater extent of Cu-depletion (<15 mg/100g) than those from below the DGTZ (<10 mg/100g; Fig. 10). Consequently the greatest depth-averaged Cu depletions occur within the sheeted dikes (Fig. 11).

Zn is mildly incompatible during magmatic fractionation and is concentrated in the glass phase, but can be incorporated into olivine, spinel, magnetite, titanomagnetite and, to a lesser extent, pyroxene (Doe, 1994). Zn behaves more variably than Cu, and absolute changes in Zn content are smaller (<6 mg/100g). The lavas are variably enriched or depleted in Zn, with no systematic difference in ΔZn of aphyric and porphyritic lava samples (Fig. 10). Within the LDTZ there is variable Zn-enrichment (< 5 mg/100g) consistent with quartz-sphalerite-chalcopyrite mineralization in this zone

(Davidson et al., 2004). Aphyric dikes record increasing Zn depletion with depth through the sheeted dike complex, to ~5 mg/100g at the DGTZ, whereas Zn is variably enriched or depleted in porphyritic dikes and gabbros in this interval (Fig. 10). Although there are no correlations between ΔS and either ΔCu or ΔZn within the Macquarie crust, ΔCu and ΔZn are weakly correlated in dike samples ($R^2 = 0.44$, $n=59$). The depletion of Cu and Zn from the aphyric dikes is consistent with previously observed base-metal losses from the lower sheeted dikes of ODP Holes 504B and 1256D due to the breakdown of sulfide minerals and titanomagnetite under greenschist facies conditions (Alt et al., 2010; Alt et al., 1996a).

The alkali elements Cs and Rb are incorporated into minerals by cation-substitution, with preferential substitution for ions of similar ionic potential. They therefore have an affinity for K-rich phases including clays and feldspars (Hart, 1969). Consequently ΔRb and ΔK_2O of Macquarie samples are correlated ($R^2 = 0.82$, $n= 203$). Rb and Cs display similar average behavior in most Macquarie lithologies except olivine gabbros, which are on average highly enriched in Rb but slightly depleted in Cs (Table 1). The anorthosites are highly enriched in Cs and Rb, which may reflect the seritization of plagioclase. The Cs and Rb enrichment of porphyritic samples relative to aphyric samples at a given depth may reflect the greater proportion of plagioclase feldspar in the aphyric samples. The observed average enrichments of K, Rb and Cs in the extrusive section are consistent with uptake from seawater during low-temperature hydrothermal alteration of in-situ upper crust (Staudigel and Hart, 1983; Teagle et al., 1996). The depletion of Rb and Cs in the lower sheeted dikes and upper gabbros (Fig. 10) is

consistent with their enrichment in hydrothermal fluids relative to both MORB and seawater (Palmer and Edmond, 1989; Von Damm, 1995).

The alkali earth elements Sr and Ba have an affinity for Ca, and Sr is therefore predominantly incorporated into Ca-rich phases such as feldspar, calcium carbonate, prehnite, and epidote. Sr is variably enriched or depleted throughout the Macquarie crust (Fig. 10). This variability reflects differences in the secondary mineral assemblages, with samples that contain significant volumes of calcium carbonate or epidote having gained Sr. On average Sr is slightly depleted in the aphyric lavas and dikes, but slightly to highly enriched in gabbro, olivine gabbro and anorthosite. Consequently, Sr is on average depleted or within error of zero change through the extrusive section and sheeted dikes, but enriched or within error of zero change through the lower crust (Fig. 11). This indicates that hydrothermal circulation caused a net transfer of Sr downward within the crust. Ba displays similar behavior to Sr on average in most Macquarie lithologies (Table 1) but unlike Sr, Ba is moderately enriched in porphyritic lavas and is therefore on average enriched through the upper 500 m of the crust (Fig. 11).

Uranium is variably enriched or depleted throughout the Macquarie crust (Fig. 10), and the depth-averaged changes in U content are within error of zero throughout most of the crustal section, with significant U-enrichment (<0.025 mg/100g) occurring only in the lavas (0-100 m and 400-500 m) as a result of U-uptake from cold seawater. U is depleted on average in the Macquarie lower lavas and upper sheet dikes, by up to 0.02 mg/100g, indicating U-loss during higher temperature fluid-rock reaction. In contrast,

the lower lavas and upper sheeted dikes of ODP Hole 504B were enriched in U under greenschist facies conditions (Bach et al., 2003). Calculated values of ΔLa and ΔLu are typically small relative to the computational uncertainty for the majority of samples (Fig. 10), consistent with previous observations that the rare earth elements are generally immobile during hydrothermal alteration of in-situ ocean crust (Bach et al., 2003; Teagle et al., 1996).

7. Elemental exchange fluxes for Macquarie Island

To assess the contribution hydrothermal alteration of the Macquarie crust made to global geochemical cycles the calculated changes in composition of the Macquarie crust due to hydrothermal alteration are converted into net fluxes to or from the crust, following:

$$F_i = \sum_t^T \Delta \bar{m}_{i-t} z_t \rho_c \quad (4)$$

Where F_i is the mass flux of component i through 1 m^2 of seafloor due to alteration of a section of crust of thickness T and $\Delta \bar{m}_{i-t}$ is the average change in mass of component i per unit mass of rock in each sub-interval t , z_t is the thickness of each sub-interval t and ρ_c is the density of the crust (2900 kg/m^3). The net fluxes due to hydrothermal alteration of the Macquarie lavas, LDTZ, sheeted dikes and gabbros, are determined from the depth-averaged Δm_i (Table S7), with uncertainty propagated from the standard error of the mean chemical change of each sub-interval (Supplementary Material). However, to fully account for the fluxes associated with hydrothermal alteration we also need to include the contribution from the veins that formed from fluids circulating through fractures in the crust.

Veins were deliberately excluded from the whole rock samples, as they need to be included in a manner representative of their true proportion within the crust, rather than individual samples. Unfortunately it is not possible to accurately estimate the proportion of the Macquarie crust that veins make up without drill core. However the volume and mineralogy of hydrothermal veins have been quantitatively logged in sections of ocean crust recovered by scientific ocean drilling. We therefore estimate the volume proportions of the various secondary vein-filling minerals through the Macquarie crust from their occurrence in representative drilled sections of ocean crust (Table 2). These data are combined with published major element analyses of secondary mineral compositions (Table 2) to estimate the net effect of hydrothermal vein formation in the Macquarie crust on global geochemical cycles. Assuming that the veins formed in open fractures, the net mass flux of component i through 1m^2 of seafloor due to hydrothermal vein formation in crustal interval T is given by:

$$F_{i-v} = z_T \sum_x V_x \rho_x M_{i-x} \quad (5)$$

where z_T is the thickness of interval T , V_x is the volume proportion of the rock filled with vein mineral x , ρ_x is the specific gravity of mineral x , and M_{i-x} is the mass proportion of component i in vein mineral x . The net uptake of major elements as a result of vein formation in the Macquarie lavas, LDTZ, sheeted dikes and gabbro are calculated using equation 5. The net mass flux of component i through 1m^2 of seafloor due to hydrothermal alteration of crustal interval T is given by combining Equations 4 and 5:

$$F_{i-TOTAL} = F_{i-v} + (1-V).F_i \quad (6)$$

where V is the total volume proportion of veins in interval T . The hydrothermal fluxes due to alteration of the Macquarie Island lavas, LDTZ, sheeted dikes and gabbros calculated using Equation 6 (Table S7) are extrapolated to global annual fluxes (Table 3), assuming a global ocean crustal production rate of $\sim 3 \text{ km}^2/\text{yr}$ (Müller et al., 2008).

8. Global Hydrothermal Fluxes

The ultimate goal of this and similar studies is to quantify the hydrothermal contributions from seawater-ocean crust exchange to global biogeochemical cycles, and assess how they have varied in the past. Hydrothermal fluxes between a given section of crust and the overlying ocean depend on the crust's age, architectural and thermal history, and the spreading rate. Consequently hydrothermal contributions to global geochemical cycles depend on the global length of slow, intermediate and fast spreading ridges and the age-area distribution of the ridge flanks, all of which have varied significantly throughout the Phanerozoic (Müller et al., 2008). To achieve this goal we therefore require complete sections of altered ocean crust produced at different spreading rates and at different times.

Several studies have quantified the chemical changes associated with hydrothermal alteration from sections of ocean crust, recovered through scientific ocean drilling of in-situ crust or tectonically uplifted lower crust, and sampling of crust tectonically exposed on the seafloor or sub-aerially exposed in ophiolites (for example, Bach et al., 2003; Bednarz and Schmincke, 1989; Coogan and Dosso, 2012; Gillis and Robinson, 1990; Staudigel, 2014). These studies vary in many ways, including: (i) the properties of the section studied, including: spreading rate, age, depth interval, and its thermal,

architectural, and hydrogeologic evolution; (ii) the elements investigated; (iii) the assumptions and numerical approaches used to compute chemical changes; (iv) the parameters used to extrapolate calculated chemical changes to global hydrothermal fluxes; and (v) their assessment of the uncertainties involved. Unfortunately our current sampling of in-situ ocean crust is too sparse to make a detailed assessment of the variations in hydrothermal fluxes with respect to spreading rate and crustal age, and a full comparison of the results of the sections sampled to date is beyond the scope of this investigation.

Here we compare the global hydrothermal fluxes extrapolated from chemical changes through the Macquarie crust with: (i) fluxes determined from hydrothermal chemical changes through a composite section of ocean crust recovered by scientific ocean drilling (Staudigel, 2014); and (ii) fluxes extrapolated from element/heat ratios of sampled hydrothermal fluids and estimates of the total convective heat loss (Elderfield and Schulz (1996) (Table 4). The altered sections of ocean crust provide time-integrated records of hydrothermal alteration, and hence should be comparable to the net axial and ridge flank fluxes (Fig. 12).

The chemical changes for the composite section of ocean crust are primarily based on analyses of in-situ lavas from DSDP Holes 417D and 418A (120 Ma, slow-spread crust; (Donnelly et al., 1979)) and tectonically uplifted gabbros from ODP Hole 735B; (9 Ma, ultraslow-spread crust (Dick et al., 1999)). Although in-situ sheeted dikes were recovered from in-situ crust at ODP Site 504 (6.9 Ma, intermediate-spread crust (Alt et al., 1996b)), the chemical changes at intermediate depths in the composite section were

in most cases extrapolated from analyses of Site 417/418 lavas and 735B gabbros because Site 504 was considered to be too young to represent hydrothermally mature ocean crust (Staudigel, 2014). Such an approach ignores the significant differences between the hydrothermal processes and hence chemical reactions occurring in the dikes compared to both the lavas and the lower crust. The composite section was therefore produced at a similar (slow) spreading rate to the Macquarie crust. Uncertainties in the estimated chemical changes are only quoted for the upper 600 m of lavas in the composite section (Staudigel, 2014), hence the uncertainties in the extrapolated annual hydrothermal fluxes (Table 4; Fig. 12) are not known.

Differences between the average chemical changes recorded by the two crustal sections likely reflect (i) differences in their stratigraphy, predominantly due to the greater thickness of gabbro in the composite section (5000 m; (Staudigel, 2014)) compared to the Macquarie crust (1150 m; Fig. 4); (ii) the longer duration of hydrothermal exchange within the lavas of the composite section, given their greater age (120 vs 10 Ma); (iii) their differing geologic histories; and (iv) and the approaches used to calculate the chemical changes. In contrast to the Macquarie crust and sampled vent fluids, the composite crust records net fluxes of Si, Al and Ca to the crust and a net flux of Mg to the oceans (Fig. 12). The discrepancies between the two studies of slow-spread crust emphasize the need for more thorough sampling of in-situ ocean crust, a consistent approach to calculating chemical changes, and full consideration of the associated uncertainties.

Assuming that hydration is the primary cause of volatile enrichment, Macquarie-style alteration results in uptake of 1.9×10^{13} mol/year of water. In contrast hydrothermal alteration of the Macquarie crust resulted in a net flux of Si to the oceans, consistent with the observed Si-enrichment of black smoker and ridge flank vent fluids relative to seawater (Butterfield et al., 2003; Wheat and Mottl, 2000). Macquarie whole rock alteration extrapolates to a Si flux to the oceans of 9.7 to 25×10^{11} mol/year but a large proportion is compensated by vein formation, resulting in a net flux to the oceans of $3.7 \pm 7.3 \times 10^{11}$ mol/year. This is less than the estimated combined Si flux from axial vents and ridge flank exchange (Elderfield and Schultz (1996); Fig. 12).

Ti was assumed to be immobile during hydrothermal alteration of the composite crustal section ((Staudigel, 2014) Table 4). However, our results indicate that hydrothermal alteration causes a net Ti flux to the oceans of 0.8 – 2.5×10^{11} mol/year, equivalent to 3 – 8% loss of Ti from the full crustal section (Table 3). Similar Ti losses (15%) from upper crustal samples from ODP Hole 504B cannot solely be attributed to dilution through secondary mineral infilling and require Ti mobility during hydrothermal alteration (Bach et al., 2003). However, titanite is common in small amounts in chlorite veins in ODP Holes 504B and 1256D (Alt et al., 1996a; Teagle et al., 2006) and the Macquarie crust, indicating that some of the mobilized Ti is re-incorporated into veins. The titanite abundance in the drilled crustal sections is not quantified and titanite-uptake is not included in our hydrothermal flux estimates. Consequently the estimated Ti-loss from the Macquarie crust is a maximum estimate.

The hydrothermal changes in Macquarie crustal composition extrapolate to a global Mg flux of $3.3 \pm 1.1 \times 10^{12}$ mol/year into the crust, but indicate that there is no net flux of Fe or Mn into or out of the crust (Fig. 12). Our extrapolated Mg flux is comparable to the combined estimates of the axial and ridge flank Mg flux ($2.5 \pm 0.2 \times 10^{12}$ mol/yr; Elderfield and Shultz (1996)). Approximately half the Macquarie Mg-uptake occurs in the lower crust (Table 3). Most likely due to tectonic exposure of the lower crust to seawater with the greatest Mg-enrichment observed 1m from a chloritic fault zone. The timing of this alteration is uncertain, and could have occurred on axis, off axis, or during uplift. Significant Mg-enrichment of the lower crust maybe therefore be restricted to crust produced at slow spreading ridges, where amagmatic extension results in uplift and exposure of the lower crust (MacLeod et al., 2009). However, our results contrast with those from ODP Hole 735B, where low-temperature alteration of uplifted lower crust acts as a source of Mg to the oceans, rather than a sink (Bach et al., 2001). The behavior of Mg during uplift of the lower crust may depend on the timing and rate of exhumation, which affect the thermal and chemical conditions of fluid-rock interaction as indicated by differing clay mineral distributions in Holes 735B and U1309D (Nozaka et al., 2008). Penetration of cold seawater causes oxidation and Mg removal but reaction with warmer fluids leads to chlorite and smectite precipitation and Mg uptake.

The modern oceans contain $\sim 75 \times 10^{18}$ moles Mg, but the Mg concentration of seawater has increased from ~ 35 to 55 mmol/kg since the Neogene (Horita et al., 2002). Such an increase requires an average net Mg flux of $\sim 1 \times 10^{12}$ mol/yr to the oceans since 35 Ma. Global hydrothermal Mg-uptake at the upper end of our estimated range (4.3×10^{12}

mol/year) is consistent with the observed increase in Mg in seawater since the Neogene, given an estimated riverine Mg input from the continents of 5.2×10^{12} mol/year (Edmond et al., 1979). If the Mg-uptake in the Macquarie lower crust is globally representative, our results therefore indicate that Mg uptake during axial and ridge flank hydrothermal alteration is sufficient to balance the Mg-budget of the oceans, given the uncertainties involved.

Hydrothermal alteration of the Macquarie crust supplied Ca to the oceans, but provided a net sink for Na. Given our estimated Ca flux to the oceans ($4.2\text{--}5.5 \times 10^{12}$ mol/year) and a maximum axial Ca flux of 1.3×10^{12} mol/year (Elderfield and Schultz, 1996) at least two thirds of the Ca removal must occur on the ridge flanks. We estimate that hydrothermal exchange removes $3.3\text{--}5.2 \times 10^{11}$ mol/yr of K from the oceans, but it is neither a net sink nor source for Cs and Rb because their removal during high temperature reactions is compensated by uptake during low temperature alteration.

Our extrapolated flux of S to the crust ($1.9\text{--}2.7 \times 10^{11}$ mol/yr) is sensitive to the volume of vein pyrite, which accounts for three quarters of this uptake (Table 3). Bulk rock S contents combined with pyrite and anhydrite vein abundances in crust from ODP Holes 504B and 735B indicate that the S flux from the volcanic crust to the oceans (2.5×10^{12} g/yr) is approximately compensated by S uptake in the lower crust (2.1×10^{12} g/yr) (Alt, 1995b). Elderfield and Shultz (1996) estimate axial fluxes of $0.85\text{--}9.6 \times 10^{11}$ mol/year H_2S to the oceans and 8.4×10^{11} mol/year SO_4 to the crust, resulting in a net axial S flux of $3.2 \pm 4.4 \times 10^{11}$ mol/year of S to the crust. The discrepancy between the estimated axial and time integrated hydrothermal S fluxes indicate that much of the

anhydrite is either dissolved at lower temperatures on the ridge flanks, or that the paucity of anhydrite in drilled crust reflects a sampling bias due to incomplete core recovery (Alt, 1995b). Although anhydrite was not recovered from the sampled Macquarie section, gypsum (formerly anhydrite) is locally present elsewhere in the Macquarie crust (Alt et al., 2003).

For the majority of the trace elements (Zn, Sr, Rb and Cs) we find no conclusive evidence that the hydrothermal alteration crust results in a net flux either to or from the oceans. The Macquarie-based estimates of global Si and S fluxes discussed above confirm the importance of determining the contribution of hydrothermal veins (Alt, 1995a; Alt et al., 1986; Alt and Teagle, 2000). Unfortunately we do not have trace element analyses of all the hydrothermal vein minerals, so the extent to which any trace element loss from the whole rock samples is compensated by uptake in veins is not determined. In the absence of uptake by veins our results indicate a net flux of $\sim 6.5 \times 10^9$ mol/year of Cu to the oceans and $\sim 1.3 \times 10^9$ mol/year of Ba to the crust. However, given the occurrence of minor chalcopyrite (CuFeS_2) veins at least some of the Cu lost from the bulk rock is re-incorporated into veins.

9. Conclusions

Most elements were variably enriched or depleted through the Macquarie crust during hydrothermal alteration. The changes in bulk rock composition (enrichment or depletion) depend upon the secondary mineral assemblages developed, and are controlled by: (i) the modal abundances of the primary minerals in the rocks; (ii) the alteration conditions such as temperature, fluid composition, or water: rock ratios; and

(iii) the chemical behavior of the elements, such as their mobility in fluid. Consequently there are variations with depth, most notably an interval of greater fluid-rock reaction at the lava-dike transition zone where lavas and dikes are enriched in K, S, Rb, Ba, and Zn. Since the rocks provide a time-integrated record of alteration, the behavior of some elements appears complex, and initial changes during high temperature alteration may be partially or completely compensated for during later, low-temperature alteration.

The hydrothermal changes in Macquarie crustal composition are used to estimate net elemental fluxes to and from the crust. Our results indicate that hydrothermal alteration results in a net flux of Si, Ti, Al, and Ca, to the oceans, whereas the crust is a net sink for H₂O, Mg, Na, K, and S. Our results also demonstrate the importance of accounting for hydrothermal uptake in veins, which affects the seawater-ocean crust exchange budgets of Si, Fe, Mg and S. The extrapolation of the hydrothermal changes through a section of ocean crust to global hydrothermal fluxes is limited by how representative that section of crust is. The relationship between spreading rate and hydrothermal flux remains poorly known. Consequently, the approach described here needs to be applied to ocean crustal sections produced at a range of spreading rates to refine global hydrothermal flux estimates.

Acknowledgments

This research was funded by: Australian Antarctic Division Project 2327-55th ANARE, Royal Society grant 24177, and Nuffield Foundation grant NAL/00392/G to DAHT; Natural Environmental Research (NERC) – Natural History Museum CASE studentship NER/S/A/2001/063 and a Royal Society Dorothy Hodgkin Fellowship (DH100131) to

879 RMC; NERC studentship NER/S/A/2005/1347A to MH; and US National Science
880 Foundation grant OCE-9911901 to JCA. GJD acknowledges support of an Australian
881 Research Council postdoctoral fellowship and large grant, and logistical and financial
882 support from ANARE grant 2122, Mineral Resources Tasmania. We thank the crew of
883 the Aurora Australis and especially the Macquarie Island base staff, for their hospitable
884 logistical support in the field. Sincere thanks are due to Robert Connell, who
885 volunteered to companion GJD to collect Mount Waite and Double Point transect
886 samples, and gave unflagging support under often miserable conditions. Matt Cooper
887 and Andy Milton are thanked for their support with geochemical analyses. DAHT
888 acknowledges a Royal Society Wolfson Foundation Merit Award (WM130051) that
889 also supported this research.

Figure Captions

Figure 1. Summary geological map of Macquarie Island, after Goscombe and Everard (1998a) and Varne et al. (2000). Major faults interpreted to be seafloor-spreading structures are distinguished, following Wertz et al. (2003) and Daczko et al. (2005). Inset map shows the main regional tectonic features, after Kamenetsky et al. (2000).

Figure 2. Cross-sections parallel to: **(a)** the Mount Waite transect; and **(b)** the Double Point transect, after Davidson et al. (2004). Representative lava bedding and dike chilled margin orientations are indicated.

Figure 3. (a). Geological map of the Isthmus-Eagle Point transect area, after Goscombe and Everard (1998a), supplemented with our own structural measurements. Lithological and structural data are projected onto a line perpendicular to the paleo-vertical to construct a cross-section **(b)**, with reconstructed proto-Macquarie Island crustal depths indicated along this line.

Figure 4. Stratigraphic reconstruction of the proto-Macquarie Island ocean crust and depth distribution of secondary minerals. Details within the extrusive section after Goscombe and Everard (1998a). Secondary mineral distribution in upper crust after Griffin (1982), supplemented by our own observations.

Figure 5 (a) Y and Zr concentrations of Macquarie Island glasses, after Kamenetsky et al. (2000) and Wertz (2003). Group 1 glasses (black circles) comprise a suite of primitive parental magmas from which Group 2 melts (open circles) evolved as a result

of fractional crystallization. MORB glasses from a global database of spreading ridges (grey diamonds) and fracture zones (open diamonds) are shown for comparison (Jenner and O'Neill, 2012). **(b)** Comparison of Y and Zr concentrations of Macquarie Island glasses (Kamenetsky et al., 2000; Wertz, 2003) and whole rock samples.

Figure 6. Whole rock chemistry of the proto-Macquarie Island crust. Shaded area indicates the range of fresh Macquarie glass compositions, after Kamenetsky et al. (2000) and Wertz (2003).

Figure 7. Immobile element behavior during alteration. During alteration, immobile element concentrations change only in passive response to net mass loss or gain (black arrows). **(a)** If two immobile elements are similarly incompatible the magmatic fractionation crystallization trend (blue arrow) parallels the alteration trend. **(b)** If one element is compatible the magmatic and alteration trends are distinct, and the precursor composition to an altered rock is given by their intersection (e.g. altered rocks 1 and 2 have precursor compositions 1ⁱ and 2ⁱ, respectively). The variation of immobile elements in Macquarie magmas is more complex: **(c)** if both elements are incompatible the fractional crystallization of a series of primitive parental melts (produced by differing extents of partial melting) yields an array of precursor compositions (shaded region). **(d)** A similar ‘precursor array’ is produced if one element is compatible. Here altered rock 1 must have lost mass to concentrate the immobile elements, but rock 2 could be fresh or may have altered from a wide range of precursors spanning from 2’ to 2’’.

Figure 8. Comparison of (a) Zr/Y and (b) Nb/Y ratios for pairs of more- and less-altered rocks from the same precursor; glass compositions after Wertz (2003).

Figure 9. Flow chart showing the methods used to calculate precursor compositions for the different types of altered whole rock samples: (i) aphyric lavas and dikes, and plutonic rocks with fractionated magma compositions; (ii) phyric lavas and dikes; and (iii) cumulate plutonic rocks.

Figure 10. Calculated hydrothermal changes in mass of major element oxides and trace elements through the proto-Macquarie Island crust, for 100 g of precursor. Errors propagated on a sample-by-sample basis (see Supplementary Material).

Figure 11. Average hydrothermal changes in mass of major element oxides (g per 100g precursor) and trace elements (mg per 100g precursor), through the proto-Macquarie Island crust. Error bars show the standard error of the mean change in mass in each depth interval.

Figure 12. Global hydrothermal fluxes (mol/year) extrapolated from calculated hydrothermal changes in Macquarie crustal whole rock composition, excluding (white bars) and including (grey bars) estimated contributions from veins. Results are compared to: global hydrothermal fluxes extrapolated from chemical changes within a composite crustal section recovered by scientific ocean drilling (green ovals; (Staudigel, 2014)); and global fluxes through axial vents (red bars), ridge flanks (blue bars), and both combined (purple bars), after (Elderfield and Schultz, 1996).

Table Footnotes:

Table 1:

Blank = variable behavior; (+) < 10% enriched; + slightly (10-50%) enriched; ++ moderately (50-100%) enriched; +++ highly (>100%) enriched; (-) = < 10% depleted; – slightly (10-50%) depleted; – – moderately (50-100%) depleted.

Table 2:

a: average vol% of Hole 1256D inflated flows and sheet and massive flows (Wilson et al., 2003); b vol% in Hole 1256D (Teagle et al., 2006); c: vol% in Hole 735B (Dick et al., 1999); d: vol% estimated from Macquarie Island sample petrographic observations; e: median Hole 1256D vein mineral composition (Alt et al., 2010); f: mean Hole 504B secondary mineral composition (Laverne et al., 1995); g: mean Hole 504B vein and halo amphibole composition (Vanko et al., 1996); h: mean Hole 735B vein feldspar composition (Robinson et al., 2002); i: mean Hole 896A secondary Na-zeolite composition (Laverne et al., 1996); j: mean of Holes 1274A, 1268A and 1272A vein serpentine compositions (Moll et al., 2007).

Table 4:

a: average bulk chemical changes for a composite drilled ocean crustal section (Staudigel, 2014); b: average bulk chemical changes through the Macquarie crust, including vein-contributions for major elements; c: after Staudigel (2014), total crustal thickness = 7000 m; d: total crustal thickness = 2700 m; e: after Elderfield and Schulz (1996); f: Ti assumed to be immobile; - not determined.

References

- Adamson, D.A., Selkirk, P.M., Price, D.M., Selkirk, J.M., 1996. Pleistocene uplift and palaeoenvironments of Macquarie Island: evidence from palaeobeaches and sedimentary deposits. *Papers and Proceedings of the Royal Society of Tasmania* 130, 25-32.
- Alt, J.C., 1994. A sulphur isotopic profile through the Troodos ophiolite, Cyprus: primary composition and the effects of seawater hydrothermal alteration. *Geochimica et Cosmochimica Acta* 58, 1825-1840.
- Alt, J.C., 1995a. Subseafloor processes in mid-ocean ridge hydrothermal systems, in: Humphris, S.E., Zierenberg, R., Mullineaux, L., Thomson, R. (Eds.), *Seafloor hydrothermal systems*, Geophysical Monograph 91. American Geophysical Union, Washington, D.C., pp. 85-114.
- Alt, J.C., 1995b. Sulphur isotopic profile through the oceanic crust: sulphur mobility and seawater-crustal sulphur exchange during hydrothermal alteration. *Geology* 23, 585-588.
- Alt, J.C., Davidson, G.J., Teagle, D.A.H., Karson, J.A., 2003. Isotopic composition of gypsum in the Macquarie Island ophiolite: Implications for the sulfur cycle and the subsurface biosphere in oceanic crust. *Geology* 31, 549-552.
- Alt, J.C., Honnorez, J., Laverne, C., Emmermann, R., 1986. Hydrothermal alteration of a 1km section through the upper oceanic crust, Deep Sea Drilling Project Hole 504B: mineralogy, chemistry and evolution of seawater-basalt interactions. *Journal of Geophysical Research* 91, 10309-10335.
- Alt, J.C., Laverne, C., Coggon, R.M., Teagle, D.A.H., Banerjee, N.R., Morgan, S., Smith-Duque, C.E., Harris, M., Galli, L., 2010. The subsurface structure of a

1008 submarine hydrothermal system in ocean crust formed at the East Pacific Rise,
 1009 ODP/IODP Site 1256. *Geochemistry, Geophysics, Geosystems*.

1010 Alt, J.C., Laverne, C., Vanko, D.A., Tartarotti, P., Teagle, D.A.H., Bach, W., Zuleger,
 1011 E., Erzinger, J., Honnorez, J., Pezard, P.A., Becker, K., Salisbury, M.H.,
 1012 Wilkens, R.H., 1996a. Hydrothermal alteration of a section of upper oceanic
 1013 crust in the Eastern Equatorial Pacific: A synthesis of results from site 504
 1014 (DSDP legs 69, 70 and 83, and ODP legs 111, 137, 140 and 148), in: Alt, J.C.,
 1015 Kinoshita, H., Stokking, L.B., Michael, P.J. (Eds.), *Proceedings of the Ocean*
 1016 *Drilling Program, Scientific Results*, vol 148, pp. 417-434.

1017 Alt, J.C., Teagle, D.A.H., 2000. Hydrothermal alteration and fluid fluxes in ophiolites
 1018 and oceanic crust, in: Dilek, Y., Moores, E.M., Elthon, D., Nicolas, A. (Eds.),
 1019 *Ophiolites and Oceanic Crust: New Insights from Field Studies and the Ocean*
 1020 *Drilling Program. Spec. Pap.—Geol. Soc. Am.*, pp. 273–282.

1021 Alt, J.C., Teagle, D.A.H., Laverne, C., Vanko, D.A., Bach, W., Honnorez, J., Becker,
 1022 K., Ayadi, M., Pezard, P.A., 1996b. Ridge flank alteration of upper ocean crust
 1023 in the eastern Pacific: Synthesis of results for volcanic rocks of Holes 504B and
 1024 896A. *Proceedings of the Ocean Drilling Program, Scientific Results* 148, 435-
 1025 450.

1026 Armstrong, R.A., Kohn, B., Goscombe, B.D., Everard, J.L., 2004. U-Pb and fission
 1027 track ages from oceanic crust at Macquarie Island, 17th Australian Geological
 1028 Convention abstracts volume. Geological society of Australia.

1029 Bach, W., Alt, J.C., Niu, Y., Humphris, S.E., Erzinger, J., Dick, H.J.B., 2001. The
 1030 geochemical consequences of late-stage low-grade alteration of lower ocean

- 1031 crust at the SW Indian Ridge: results from ODP Hole 735B (Leg 176).
- 1032 *Geochimica et Cosmochimica Acta* 65, 3267-3287.
- 1033 Bach, W., Peucker-Ehrenbrink, B., Hart, S.R., Blusztajn, J., 2003. Geochemistry of
- 1034 hydrothermally altered oceanic crust: DSDP/ODP Hole 504B - Implications for
- 1035 seawater-crust exchange budgets and Sr- and Pb-isotopic evolution of the
- 1036 mantle. *Geochemistry, Geophysics, Geosystems* 4, doi:10.1029/2002GC000419.
- 1037 Bednarz, U., Schmincke, H.U., 1989. Mass transfer during sub-seafloor alteration of the
- 1038 upper Troodos crust (Cyprus). *Contributions to Mineralogy and Petrology* 102,
- 1039 93-101.
- 1040 Bednarz, U., Schmincke, H.U., 1991. Chemical patterns of seawater and hydrothermal
- 1041 alteration in the northeastern Troodos extrusive series and sheeted dyke complex
- 1042 (Cyprus), in: Gibson, I.L., Malpas, J., Robinson, P.T., Xenophontos, C. (Eds.),
- 1043 Cyprus crustal study project: Initial Report, Holes CY-1 and 1a. Geological
- 1044 Survey of Canada, pp. 639-653.
- 1045 Bickle, M.J., Teagle, D.A.H., 1992. Strontium alteration in the Troodos ophiolite:
- 1046 implications for fluid fluxes and geochemical transport in mid-ocean ridge
- 1047 hydrothermal systems. *Earth and Planetary Science Letters* 113, 219-237.
- 1048 Blackman, D.K., Ildefonse, B., John, B.E., Ohara, Y., Miller, D.J., MacLeod, C.J., and
- 1049 the Expedition 304/305 Scientists, 2006. Proceedings of the Integrated Ocean
- 1050 Drilling Program, 304/305. Integrated Ocean Drilling Program Management
- 1051 International, Inc, College Station, TX.
- 1052 Brewer, T.S., Daly, J.S., Åhäll, K.-I., 1998. Contrasting magmatic arcs in the
- 1053 Palaeoproterozoic of the south-western Baltic Shield. *Precambrian Research* 92,
- 1054 297–315.

- 1055 Butterfield, D.A., Seyfried, W.E., Lilley, M.D., 2003. Compostion and evolution of
1056 hydrothermal fluids, in: Halbech, P.E., Tunncliffe, V., Hein, J.R. (Eds.), Energy
1057 and mass transfer in marine hydrothermal systems. Dahlem University Press,
1058 Berlin, pp. 123-161.
- 1059 Cande, S.C., Stock, J.M., Muller, R.D., Ishihara, T., 2000. Cenozoic motion between
1060 East and West Antarctica. *Nature* 404, 145-150.
- 1061 Cannat, M., 1996. How thick is the magmatic crust at slow spreading oceanic ridges?
1062 *Journal of Geophysical Research* 101, 2847-2857.
- 1063 Cannat, M., Sauter, D., Bezos, A., Meyzen, C., Humler, E., Le Rigoleur, M., 2008.
1064 Spreading rate, spreading obliquity, and melt supply at the ultraslow spreading
1065 Southwest Indian Ridge. *Geochemistry, Geophysics, Geosystems* 9.
- 1066 Chen, Y.J., 1992. Oceanic crustal thickness versus spreading rate. *Geophysical*
1067 *Research Letters* 19, 753-756.
- 1068 Cocker, J.D., Griffin, B.J., Muehlenbachs, K., 1982. Oxygen and carbon isotope
1069 evidence for seawater hydrothermal alteration of the Macquarie-Island ophiolite.
1070 *Earth and Planetary Science Letters* 61, 112-122.
- 1071 Coogan, L.A., Dosso, S., 2012. An internally consistent, probabilistic, determination of
1072 ridge-axis hydrothermal fluxes from basalt-hosted systems. *Earth and Planetary*
1073 *Science Letters* 323-324, 92-101.
- 1074 Daczko, N.R., Mosher, S., Coffin, M.F., Meckel, T.A., 2005. Tectonic implications of
1075 fault-scarp-derived volcanoclastic deposits on Macquarie Island: Sedimentation
1076 at a fossil ridge-transform intersection? *Bulletin of the Geological Society of*
1077 *America* 117, 18-31.

- 1078 Davidson, G.J., Varne, R., Brown, A.V., Connell, R., 2004. Structural controls on
1079 sulphide deposition at the dyke-lava boundary, slow-spreading ocean crust,
1080 Macquarie Island. *Terra Nova* 16, 9-15.
- 1081 Dick, H.J.B., Lin, J., Schouten, H., 2003. An ultraslow-spreading class of ocean ridge.
1082 *Nature* 426, 405-412.
- 1083 Dick, H.J.B., Natland, J.H., Ildefonse, B., 2006. Past and Future Impact of Deep
1084 Drilling in the Oceanic Crust and Mantle. *Oceanography* 19, 72-80.
- 1085 Dick, H.J.B., Natland, J.H., Miller, D.J., the ODP Leg 176 Shipboard Party, 1999.
1086 Proceedings of the Ocean Drilling Program, Initial Report, vol 176. Ocean
1087 Drilling Program, College Station, TX.
- 1088 Dijkstra, A., Cawood, P.A., 2004. Base-up growth of ocean crust by multiple phases of
1089 magmatism: field evidence from Macquarie Island. *Journal of the Geological*
1090 *Society, London* 161, 739-742.
- 1091 Doe, B.R., 1994. Zinc, copper, and lead in mid-ocean ridge basalts and the source rock
1092 control on Zn/Pb in ocean-ridge hydrothermal deposits. *Geochimica et*
1093 *Cosmochimica Acta* 58, 2215-2223.
- 1094 Donnelly, T., Francheteau, J., Bryan, W., Robinson, P.T., Flower, M., Salisbury, M.,
1095 1979. Init. Rept. DSDP, Washington, DC.
- 1096 Duncan, R.A., Varne, R., 1988. The age and distribution of the igneous rocks of
1097 Macquarie Island. *Papers and Proceedings of the Royal Society of Tasmania*
1098 122, 45-50.
- 1099 Edmond, J.M., Measures, C.I., McDuff, R.E., Chan, L.H., Collier, R., et al., 1979.
1100 Ridge crest hydrothermal activity and the balance of the major and minor

1101 elements in the ocean: the Galapagos data. *Earth and Planetary Science Letters*
 1102 46, 1-18.

1103 Elderfield, H., Schultz, A., 1996. Mid-ocean ridge hydrothermal fluxes and the
 1104 chemical composition of the ocean. *Annual Review of Earth and Planetary*
 1105 *Sciences* 24, 191-224.

1106 Gillis, K.M., Robinson, P.T., 1990. Patterns and processes of alteration in the lavas and
 1107 dikes of the Troodos ophiolite, Cyprus. *Journal of Geophysical Research* 95,
 1108 21523-21548.

1109 Goscombe, B.D., Everard, J.L., 1998a. *Geology of Macquarie Island. Mineral*
 1110 *Resources Tasmania*, Hobart, Australia.

1111 Goscombe, B.D., Everard, J.L., 1998b. Macquarie Island mapping reveals three tectonic
 1112 phases. *EOS, Transactions of the American Geophysical Union* 80, 50-55.

1113 Goscombe, B.D., Everard, J.L., 2001. Tectonic evolution of Macquarie Island:
 1114 extensional structures and block rotations in oceanic crust. *Journal of Structural*
 1115 *Geology* 23, 639-673.

1116 Grant, J.A., 1982. The isocon diagram - A simple solution to Gresens' Equation for
 1117 metasomatic alteration. *Economic Geology* 81, 1976-1982.

1118 Gregory, R.T., Taylor, H.P., 1981. An oxygen isotope profile in a section of cretaceous
 1119 oceanic crust, Semail Ophiolite, Oman: Evidence for $d^{18}O$ buffering of the
 1120 oceans by deep (>5km) seawater-hydrothermal circulation at mid-ocean ridges.
 1121 *Journal of Geophysical Research-Solid Earth* 86, 2737-2755.

1122 Gresens, R.L., 1967. Composition-volume relationships of metasomatism. *Chemical*
 1123 *Geology* 2, 47-65.

- 1124 Griffin, B.J., 1982. Igneous and metamorphic petrology of lavas and dykes of the
1125 Macquarie Island ophiolite complex. Ph.D. thesis. University of Tasmania,
1126 Hobart.
- 1127 Griffin, B.J., Varne, R., 1980. The Macquarie Island ophiolite complex: Mid-Tertiary
1128 oceanic lithosphere from a major ocean basin. *Chemical Geology* 30, 258-308.
- 1129 Hart, S.R., 1969. K, Rb, Cs contents and K/Rb, K/Cs ratios of fresh and altered
1130 submarine basalts. *Earth and Planetary Science Letters* 6, 295-303.
- 1131 Horita, J., Zimmerman, H., Holland, H.D., 2002. Chemical evolution of seawater during
1132 the Phanerozoic: Implications from the record of marine evaporites. *Geochimica
1133 et Cosmochimica Acta* 66, 3733-3756.
- 1134 Jenner, F.E., O'Neill, H.S.C., 2012. Analysis of 60 elements in 616 ocean floor basaltic
1135 glasses. *Geochemistry, Geophysics, Geosystems* 13.
- 1136 Kamenetsky, V.S., Everard, J.L., Crawford, A.J., Varne, R., Eggins, S.M., Lanyon, R.,
1137 2000. Enriched end-member of primitive MORB melts: petrology and
1138 geochemistry of glasses from Macquarie Island (SW Pacific). *Journal of
1139 Petrology* 41, 411-430.
- 1140 Kamenetsky, V.S., Maas, R., 2002. Mantle-melt evolution (dynamic source) in the
1141 origin of a single MORB suite: A perspective from magnesian glasses of
1142 Macquarie Island. *Journal of Petrology* 43, 1909-1922.
- 1143 Lamarche, G., Collot, J.Y., Wood, R.A., Sosson, M., Sutherland, R., Delteil, J., 1997.
1144 The Oligocene-Miocene Pacific-Australia plate boundary, south of New
1145 Zealand: Evolution from oceanic spreading to strike-slip faulting. *Earth and
1146 Planetary Science Letters* 148, 129-139.

- 1147 Laverne, C., Belarouchi, A., Honnorez, J., 1996. Alteration mineralogy and chemistry
1148 of the upper oceanic crust from Hole 896A, Costa Rica Rift, in: Alt, J.C.,
1149 Kinoshita, H., Stokking, L.B., Michael, P.J. (Eds.), Proceedings of the Ocean
1150 Drilling Program, Scientific Results, vol 148, pp. 151-169.
- 1151 Laverne, C., Vanko, D.A., Tartarotti, P., Alt, J.C., 1995. Chemistry and
1152 geothermometry of secondary minerals from the deep sheeted dike complex,
1153 Hole 504B. , in: Erzinger, J., Becker, K., Dick, H.J.B., Stokking, L.B. (Eds.),
1154 Proceedings of the Ocean Drilling Program, Scientific Results, vol 148. Ocean
1155 Drilling Program, College Station, TX pp. 167-189.
- 1156 Lechler, P.J., Desilets, M.O., 1987. A review of the use of loss on ignition as a
1157 measurement of total volatiles in whole-rock analysis. Chemical Geology 63,
1158 341-344.
- 1159 Lewis, S.J., 2007. Focussed hydrothermal alteration in upper crustal oceanic faults on
1160 Macquarie Island. PhD thesis. University of Tasmania.
- 1161 MacLean, W.H., 1990. Mass change calculations in altered rock series. Mineralium
1162 Deposita 25, 44-49.
- 1163 MacLean, W.H., Barrett, T.J., 1993. Lithogeochemical techniques using immobile
1164 elements. Journal of Geochemical Exploration 48, 109-133.
- 1165 MacLeod, C.J., Searle, R.C., Murton, B.J., Casey, J.F., Mallows, C., S.C., U.,
1166 Achenbach, K.L., Harris, M., 2009. Life cycle of oceanic core complexes. Earth
1167 and Planetary Science Letters 287, 333-344.
- 1168 Massell, C., Coffin, M.F., Mann, P., Mosher, S., Frohlich, C., Duncan, C.S., Karner, G.,
1169 Ramsay, D., Lebrun, J.F., 2000. Neotectonics of the Macquarie Ridge Complex,

- 1170 Australia-Pacific plate boundary. *Journal of Geophysical Research-Solid Earth*
1171 105, 13457-13480.
- 1172 Miyashiro, A., 1973. The Troodos ophiolite complex was probably formed in an island
1173 arc. *Earth and Planetary Science Letters* 19, 218-224.
- 1174 Moll, M., Paulick, H., Suhr, G., Bach, W., 2007. Data report: Microprobe analyses of
1175 primary phases (olivine, pyroxene, and spinel) and alteration products
1176 (serpentine, iowaite, talc, magnetite, and sulfides) in Holes 1268A, 1272A, and
1177 1274A., in: Kelemen, P.B., Kikawa, E., Miller, D.J. (Eds.), *Proceedings of the*
1178 *Ocean Drilling Program, Scientific Results*, vol 209. Ocean Drilling Program,
1179 College Station, TX.
- 1180 Müller, R.D., Sdrolias, M., Gaina, C., Steinberger, B., Heine, C., 2008. Long-Term Sea
1181 Level Fluctuations Driven by Ocean Basin Dynamics. *Science* 319, 1357-1362.
- 1182 Norrish, K., Hutton, J.T., 1969. An accurate X-ray spectrographic method for the
1183 analysis of a wide range of geological samples. *Geochimica et Cosmochimica*
1184 *Acta* 33, 431 453.
- 1185 Nozaka, T., Fryer, P., Andreani, M., 2008. Formation of clay minerals and exhumation
1186 of lower-crustal rocks at Atlantis Massif, Mid-Atlantic Ridge. *Geochem.*
1187 *Geophys. Geosys.* 9, Q11005.
- 1188 Palmer, M.R., Edmond, J.M., 1989. Cesium and rubidium in submarine hydrothermal
1189 fluids: evidence for recycling of alkali elements. *Earth and Planetary Science*
1190 *Letters* 95, 8-14.
- 1191 Penrose Conference Participants, 1972. Report of the Penrose field conference on
1192 ophiolites. *Geotimes* 17, 24-25.

- 1193 Portner, R.A., Murphy, M.J., Daczko, N.R., 2010. A detrital record of lower oceanic
1194 crust exhumation within a Miocene slow-spreading ridge: Macquarie Island,
1195 Southern Ocean. *Geological Society of America Bulletin* 123, 255–273.
- 1196 Quilty, P.G., Crundwell, M.P., Wise Jr, S.W., 2008. Microplankton provide 9 Ma age
1197 for sediment in the Macquarie Island ophiolite complex. *Australian Journal of*
1198 *Earth Sciences* 55, 1119-1125.
- 1199 Rautenschlein, M., Jenner, G.A., Hertogen, J., Hofmann, A.W., Kerrich, R., Schmincke,
1200 H.U., White, W.M., 1985. Isotopic and trace element composition of volcanic
1201 glasses from the Akaki Canyon, Cyprus: Implications for the origin of the
1202 Troodos ophiolite. *Earth and Planetary Science Letters* 75, 369-383.
- 1203 Rivizzigno, P.A., Karson, J.A., 2004. Structural expression of oblique seafloor
1204 spreading in the Macquarie Island Ophiolite, Southern Ocean. *Geology* 32, 125-
1205 128.
- 1206 Robinson, P.T., Erzinger, J., Emmermann, R., 2002. The Composition and Origin of
1207 Igneous and Hydrothermal Veins in the Lower Ocean Crust—ODP Hole 735B,
1208 Southwest Indian Ridge, in: Natland, J.H., H.J.B., D., Miller, D.J., Von Herzen,
1209 R.P. (Eds.), *Proceedings of the Ocean Drilling Program, Scientific Results*, vol
1210 176. Ocean Drilling Program, College Station (TX).
- 1211 Robinson, P.T., Von Herzen, R., the ODP Leg 118 Shipboard Party, 1989. *Proceedings*
1212 *of the Ocean Drilling Program, Initial Reports*, vol 118. Ocean Drilling Program,
1213 College Station, TX.
- 1214 Selkirk, P.M., Seppelt, R.D., Selkirk, D.R., 1990. Subantarctic Macquarie Island:
1215 Environment and biology. Cambridge University Press, Cambridge.

- 1216 Sinha, M.C., Constable, S., Peirce, C., White, A., Heinson, G., MacGregor, L.M.,
1217 Navin, D.A., 1998. Magmatic processes at slow spreading ridges: implications
1218 of the RAMESSES experiment, Mid-Atlantic Ridge at 57° N. *Geophysical*
1219 *Journal International* 135, 731-745.
- 1220 Staudigel, H., 2014. Chemical Fluxes from Hydrothermal Alteration of the Oceanic
1221 Crust, in: Rudnick, R.L. (Ed.), *Treatise on Geochemistry*, 2nd Edition, Vol 4:
1222 *The Crust*. Elsevier, Oxford, pp. 583-606.
- 1223 Staudigel, H., Hart, S.R., 1983. Alteration of basaltic glass: mechanisms and
1224 significance for the oceanic crust budget. *Geochimica et Cosmochimica Acta* 47,
1225 337-350.
- 1226 Sutherland, R., 1995. The Australian-Pacific boundary and Cenozoic plate motions in
1227 the SW Pacific: Some constraints from Geosat data. *Tectonics* 14, 819-831.
- 1228 Teagle, D., Ildefonse, B., 2011. Journey to the mantle of the Earth. *Nature* 471, 437-
1229 439.
- 1230 Teagle, D.A.H., Alt, J.C., Bach, W., Halliday, A.N., Erzinger, J., 1996. Alteration of
1231 upper ocean crust in a ridge-flank hydrothermal upflow zone: mineral, chemical,
1232 and isotopic constraints from Hole 896A., in: Alt, J.C., Kinoshita, H., Stokking,
1233 L.B., Michael, P.J. (Eds.), *Proceedings of the Ocean Drilling Program, Scientific*
1234 *Results*, vol 148. Ocean Drilling Program, College Station (TX), pp. 119-150.
- 1235 Teagle, D.A.H., Alt, J.C., Umino, S., Miyashita, S., Banerjee, N.R., Wilson, D.S., the
1236 Expedition 309/312 Scientists, 2006. Superfast spreading rate crust 2 and 3.
1237 (Integrated Ocean Drilling Program Management International, Inc)
1238 doi:10.2204/iodp.proc.309312.2006, Washington DC.

- 1239 Vanko, D.A., Laverne, C., Tartarotti, P., Alt, J.C., 1996. Chemistry and origin of
1240 secondary minerals from the deep sheeted dikes cored during Leg 148 (Hole
1241 504B), in: Alt, J.C., Kinoshita, H., Stokking, L.B., Michael, P.J. (Eds.),
1242 Proceedings of the Ocean Drilling Program, Scientific Results, vol 148. Ocean
1243 Drilling Program, College Station, TX pp. 71-86.
- 1244 Varne, R., Brown, A.V., Falloon, T., 2000. Macquarie Island: Its geology, structural
1245 history, and the timing and tectonic setting of its N-MORB to E-MORB
1246 magmatism. Geological Society of America Special Paper 349.
- 1247 Varne, R., Gee, R.D., Quilty, P.G.J., 1969. Macquarie Island and the cause of oceanic
1248 linear magnetic anomalies. *Science* 166, 230-233.
- 1249 Von Damm, K.L., 1995. Controls on the Chemistry and Temporal Variability of
1250 Seafloor Hydrothermal Fluids, in: Humphris, S.E., Zierenberg, R.A.,
1251 Mullineaux, L.S., Thompson, R.E. (Eds.), Seafloor Hydrothermal Systems,
1252 Geophysical Monograph 91. American Geophysical Union, Washington, DC,
1253 pp. 222-247.
- 1254 Wertz, K.L., 2003. From seafloor spreading to uplift: the structural and geochemical
1255 evolution of Macquarie Island on the Australian-Pacific plate boundary.
1256 University of Texas, Austin, p. 169.
- 1257 Wertz, K.L., Mosher, S., Daczko, N.R., Coffin, M.F., 2003. Macquarie Island's Finch-
1258 Langdon fault: A ridge-transform inside-corner structure. *Geology* 31, 661-664.
- 1259 Wheat, C.G., Mottl, M.J., 2000. Compositions of pore and spring waters from Baby
1260 Bare: Global implications of geochemical fluxes from a ridge flank
1261 hydrothermal system. *Geochimica et Cosmochimica Acta* 64, 629-642.

1262 Wilson, D.S., Teagle, D.A.H., Acton, G.D., and the ODP Leg 206 Shipboard Party,
1263 2003. Proceedings of the Ocean Drilling Program, Initial Reports. Ocean
1264 Drilling Program, College Station, TX.

1265

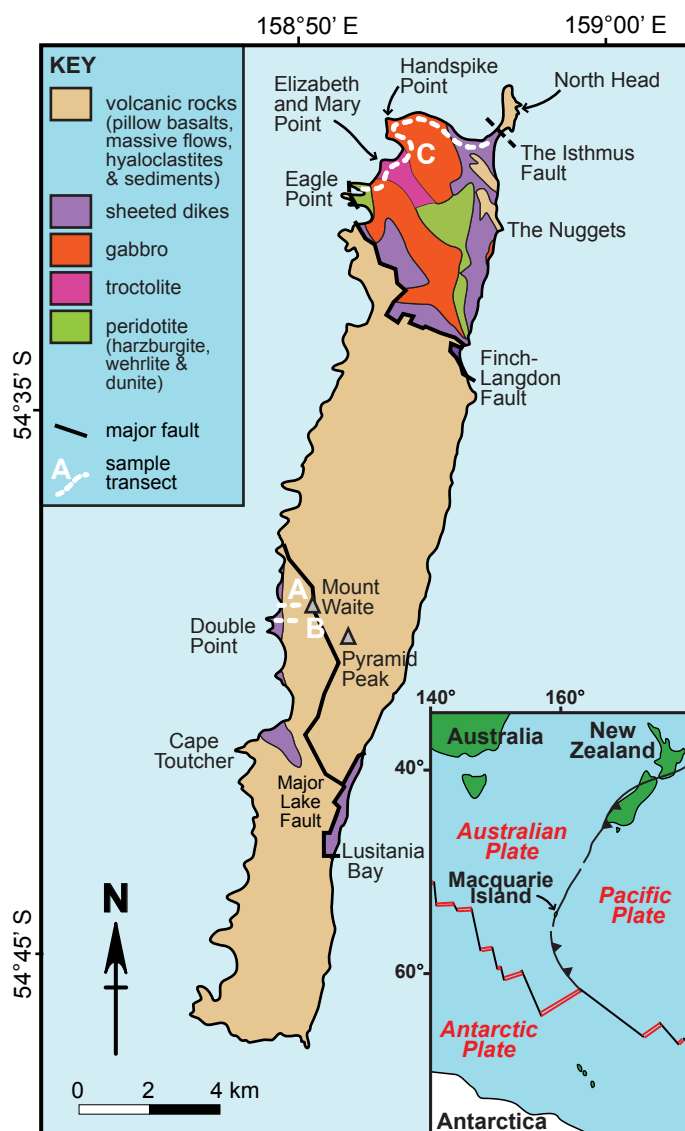


Figure 1

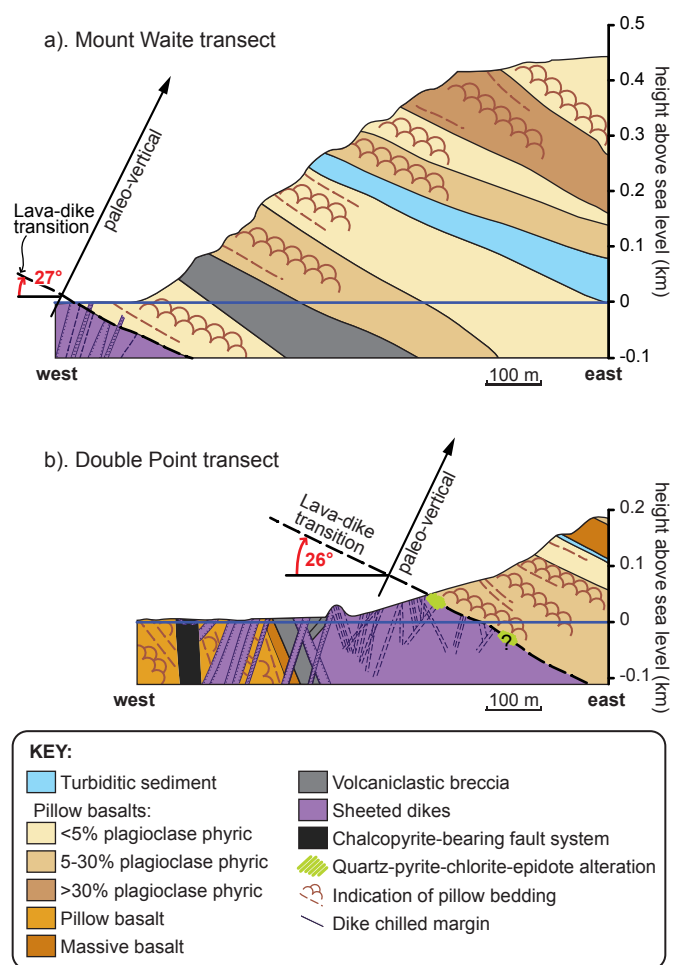


Figure 2.

Figure 3.

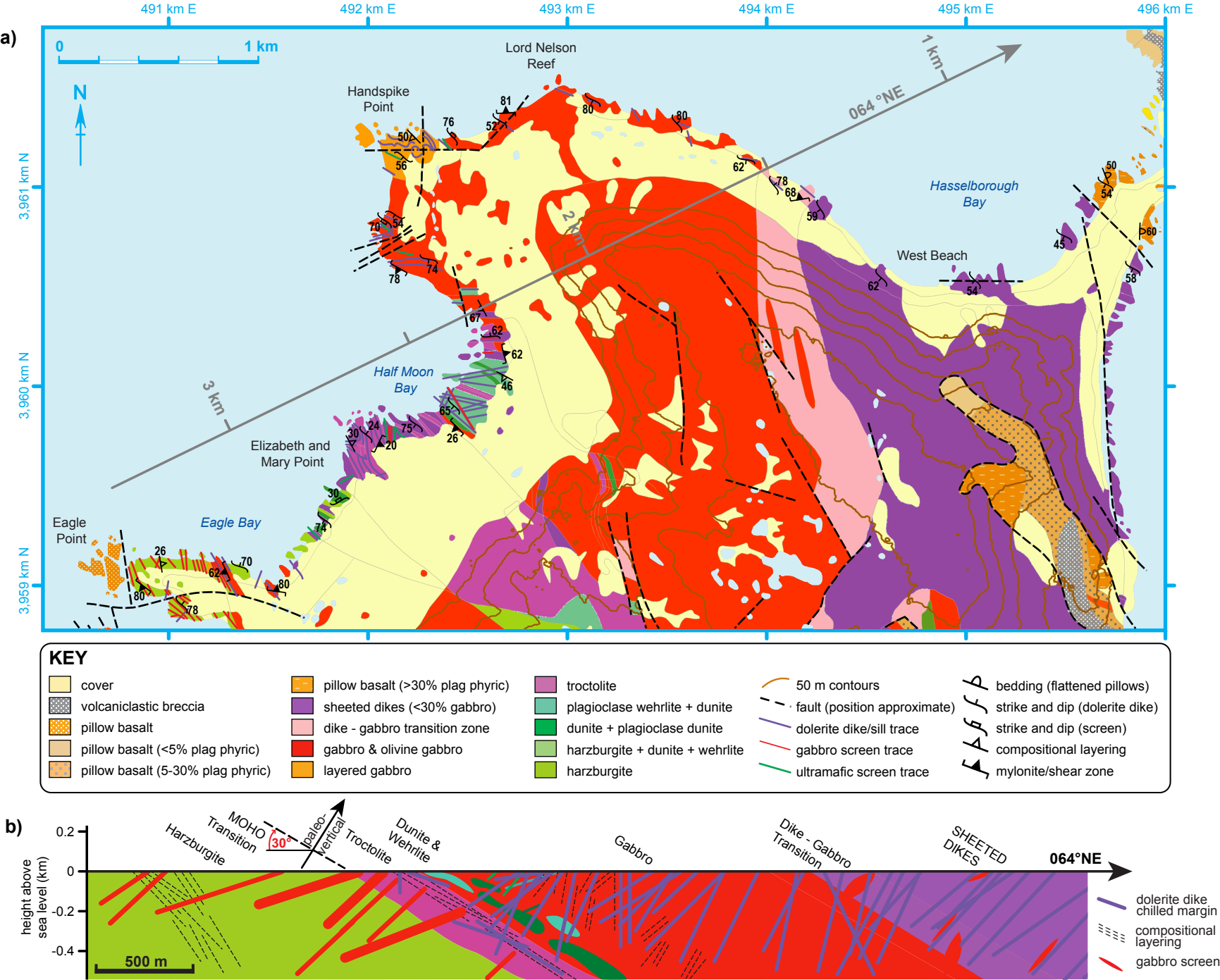


Figure 4.

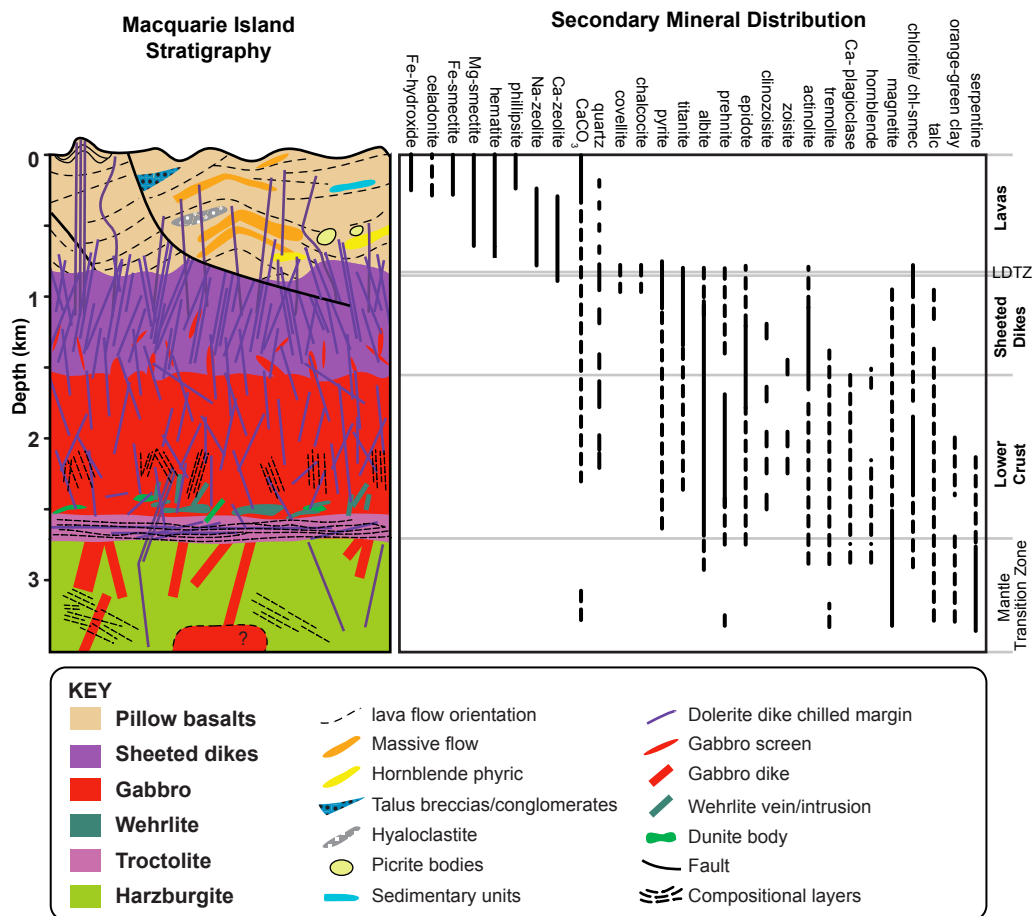


Figure 5.

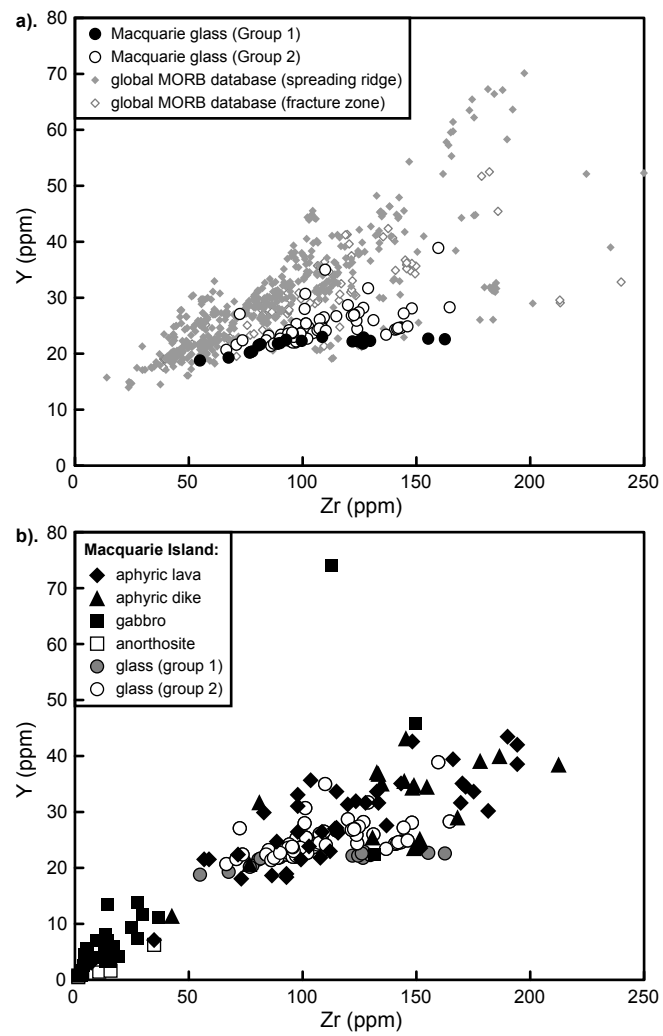


Figure 6.

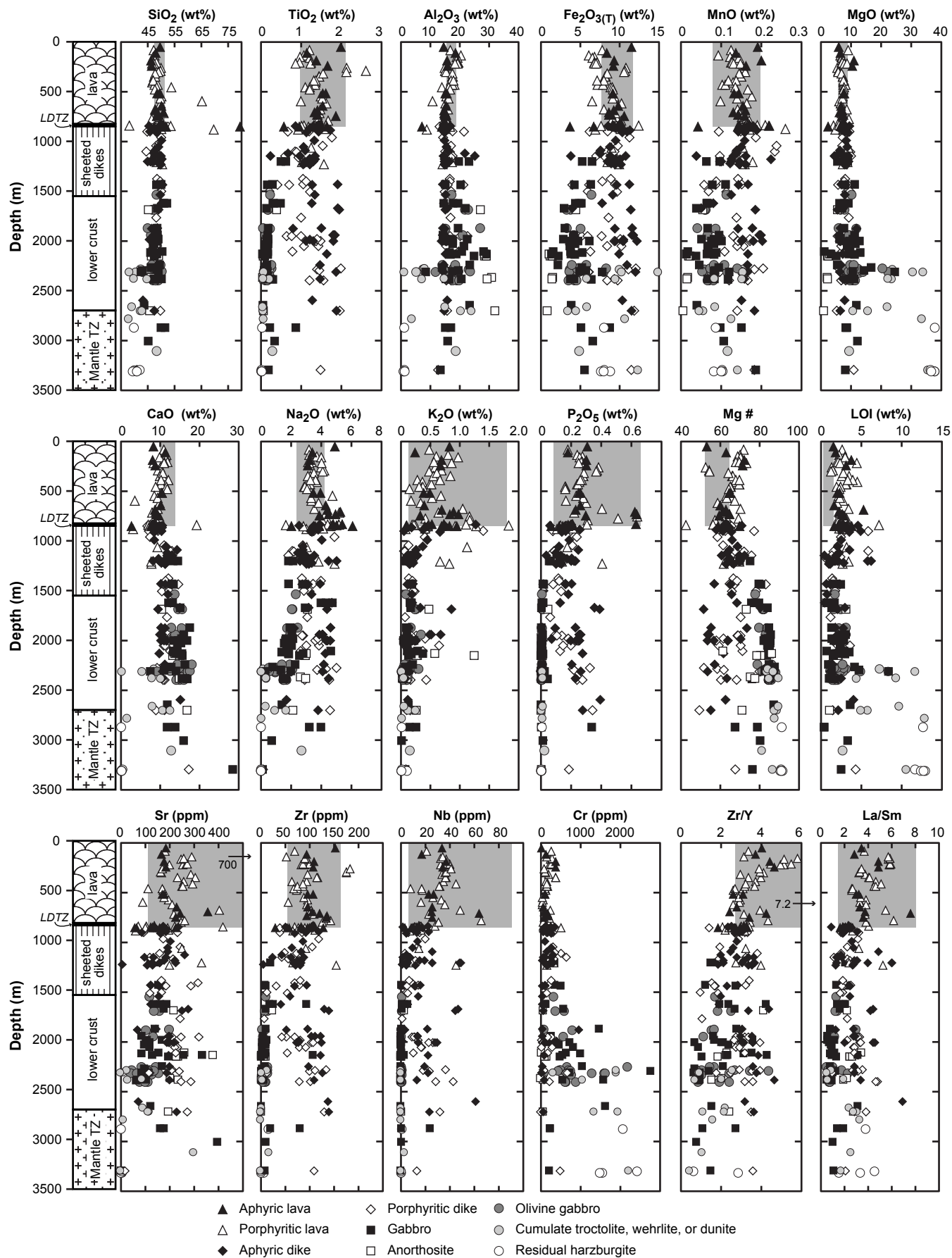


Figure 7.

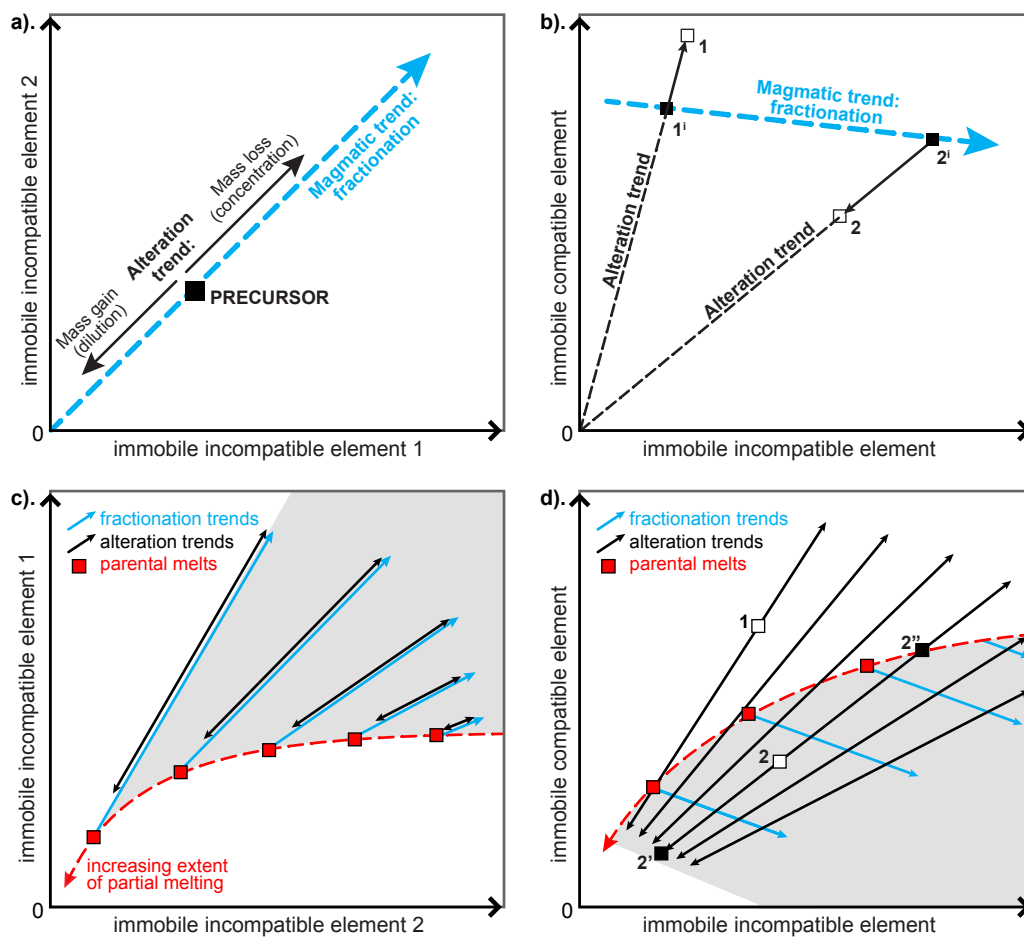


Figure 8.

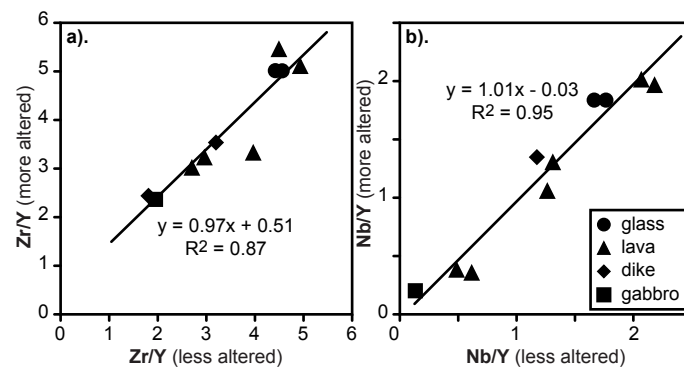


Figure 9.

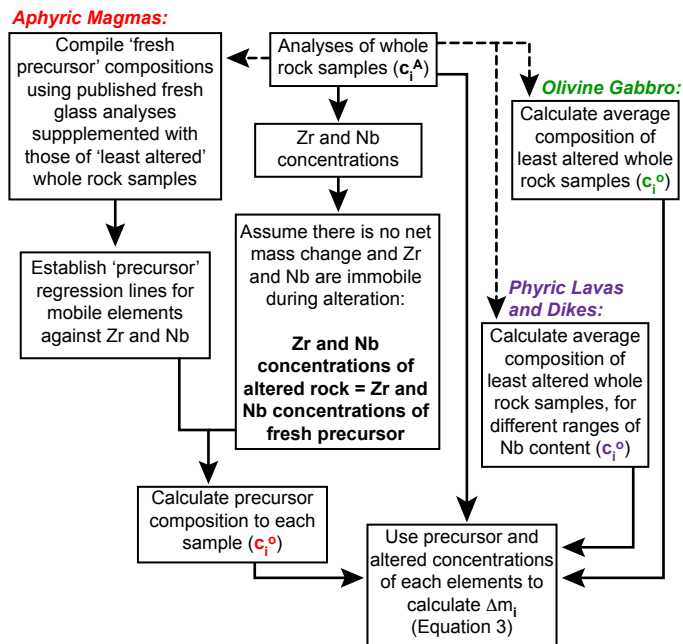


Figure 10.

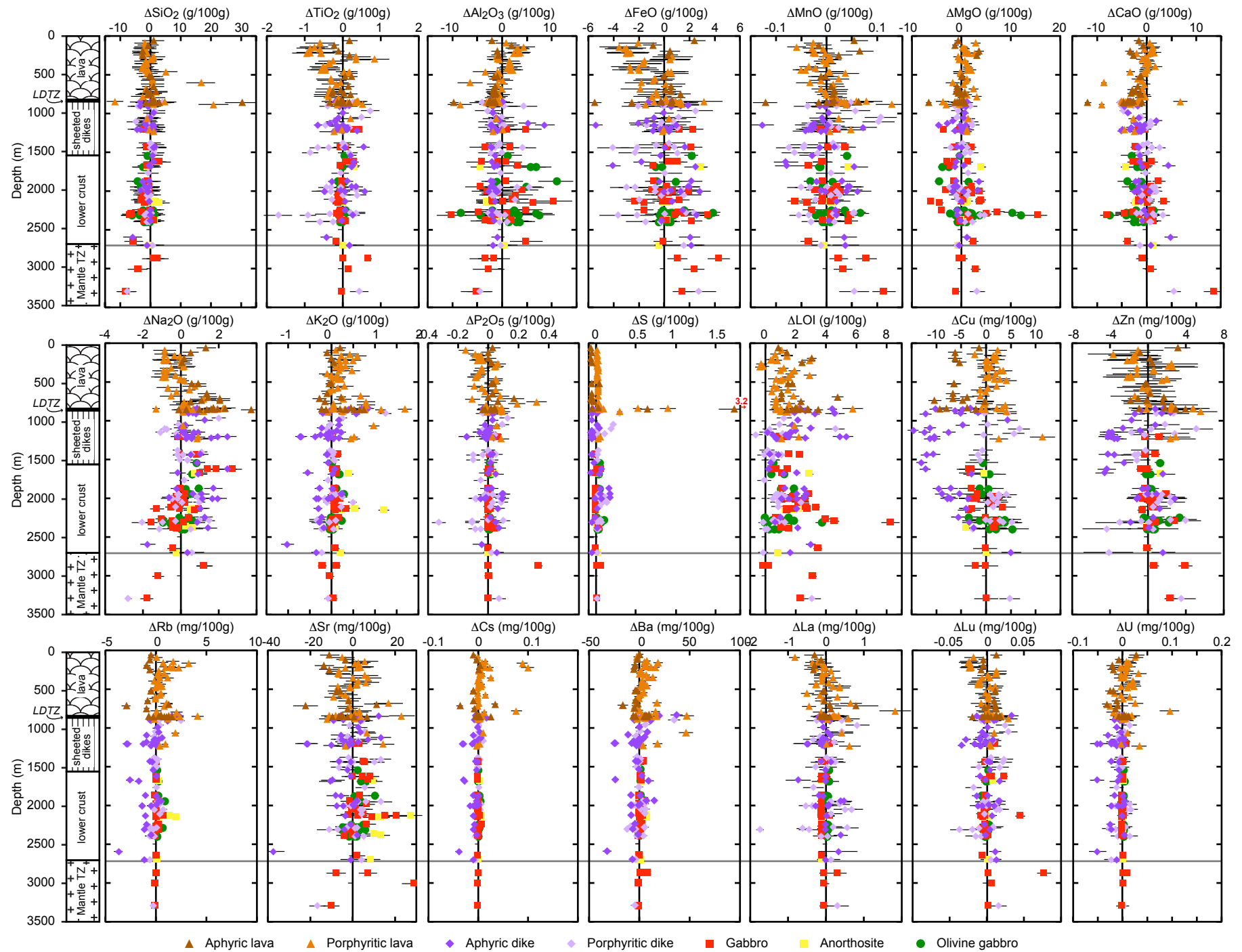


Figure 11.

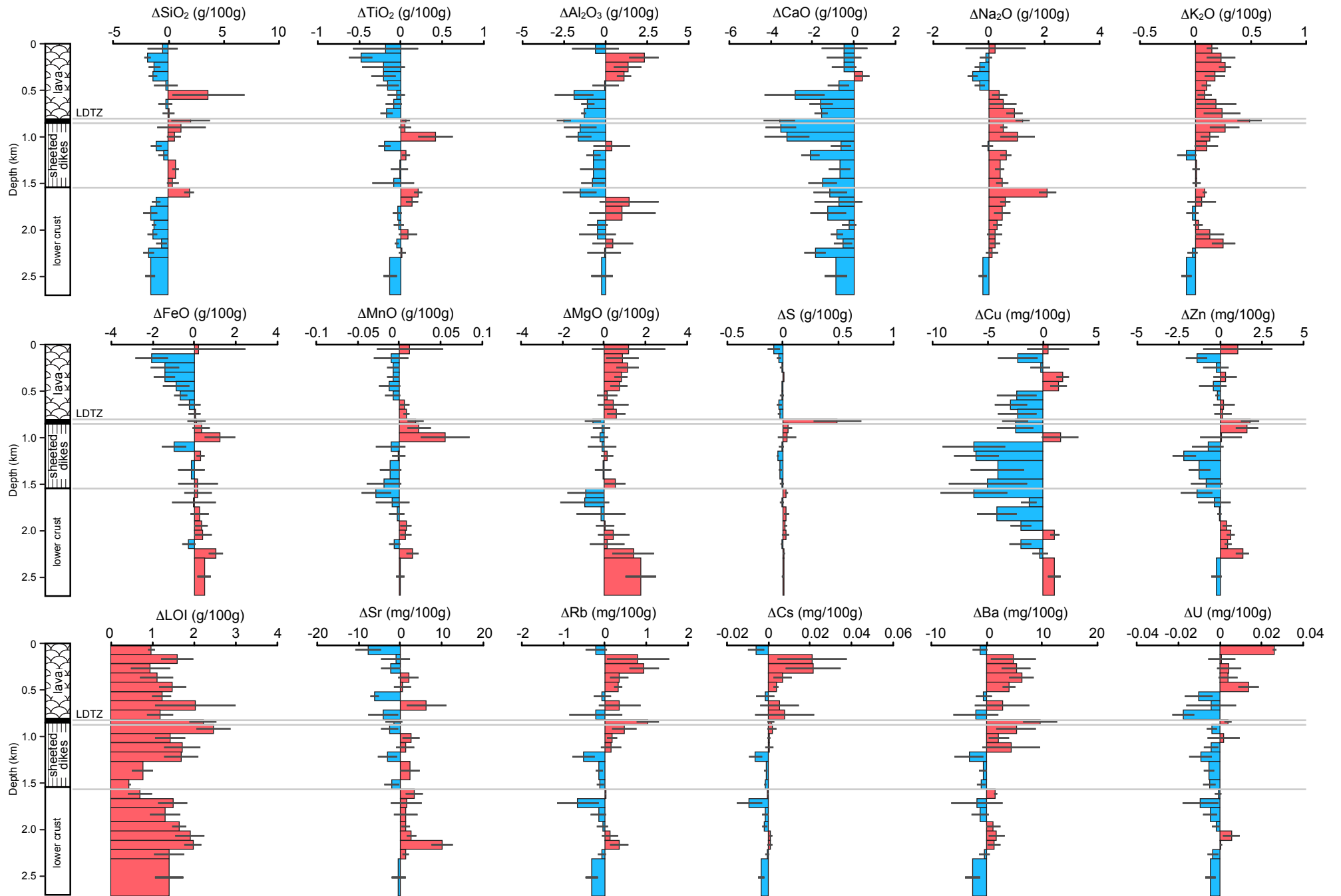


Figure 12.

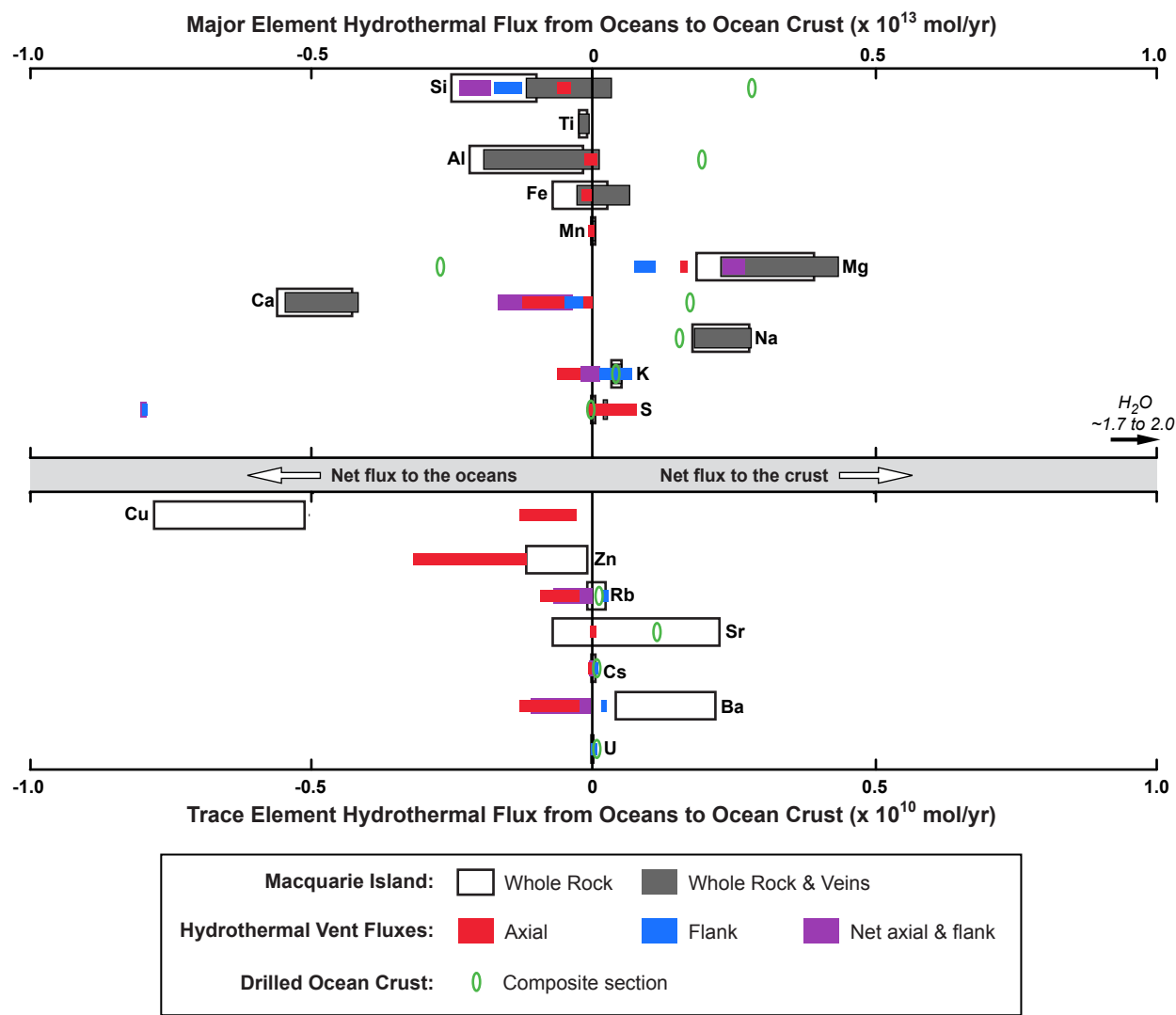


Table 1. Summary of chemical changes for each Macquarie lithology

	Lavias		Dikes		Gabbro	Anorthosite	Olivine Gabbro
	Aphyric	Porphyritic	Aphyric	Porphyritic			
SiO ₂	(+)		(-)	(-)	(-)	(+)	(-)
TiO ₂		-	(+)	(-)	+	+++	(-)
Al ₂ O ₃	-		(-)	(-)		(-)	+
FeO _T		(-)	(+)		+	+	+
MnO	(+)	(+)			(+)	++	
MgO		(+)		(+)	(+)	++	
CaO	-	-	-			(-)	-
Na ₂ O	+		+			+	
K ₂ O	+	+++	-	+	+++	+++	+
P ₂ O ₅	+				+++	+++	+++
S	+++	+++	-	+++	-		++
LOI	+++	++	+++	++	+++	+++	++
Cu	--	++	--	++	-	-	+
Zn	+	+	-	+	+	++	+
Rb	-	+++	--		++	+++	+++
Sr	-		-		+	+++	+
Cs	-	+++	--	-	+	+++	-
Ba	(-)	++	-		+	+++	+++
La			(-)		-	--	+
Lu	+				+	+++	-
U	-	+	-	-	+	++	++

Table 2. Summary of average vein mineral abundances and compositions in drill core

Vein Mineral	Specific Gravity	Vein Mineral Abundance (vol%)				Vein Mineral Composition (wt%)										Total	Reference
		Lavas ^a	LDTZ ^b	Sheeted Dikes ^b	Gabbro ^c	SiO ₂	TiO ₂	Al ₂ O ₃	FeO	Fe ₂ O ₃	MnO	MgO	CaO	Na ₂ O	K ₂ O		
Mg-saponite	2.27	0.85	0.6	0.01	0.14	47.71	0.04	5.64	15.43		0.05	16.07	0.82	0.11	0.44	86.31	e
Celadonite	3.00	0.12				51.24	0.05	3.57	23.56		0.02	4.93	0.50	0.01	7.19	91.06	e
Prehnite	2.88	0.01 ^d	0.01	0.01	0.01 ^d	42.67	0.01	22.83		2.07	0.07	0.78	24.87	0.03	0.03	93.35	f
Epidote	3.45			0.01	0.008	37.95	0.08	23.47		11.74	0.11	0.27	23.07	0.02	0.01	96.73	f
Chlorite	2.95		0.3	0.44	0.007	28.52	0.02	17.59	21.89		0.26	14.45	0.20	0.01	0.01	82.94	e
Amphibole	3.00			0.01	0.12	51.19	0.46	4.07	14.38		0.22	14.51	11.01	0.67	0.02	96.52	g
Feldspar	2.63				0.11	63.44	0.01	22.85		0.15			4.15	8.95	0.10	99.64	h
Na-zeolite	2.20	0.01	0.05			59.70		18.58	0.65			0.69	1.66	4.69	5.81	91.77	i
Serpentine					0.005 ^d	40.32	0.01	0.56	5.18			37.33	0.26			96.01	j
Mineral Formulae																	
Calcite	2.85	0.01	0.01	0.01	0.02	CaCO ₃											
Fe(O,OH)x	2.71	0.01			0.01 ^d	Fe(O,OH)											
Quartz/SiO₂	2.65	0.15	0.03	0.13	0.02	SiO ₂											
Ca-zeolite	2.29		0.05	0.01	0.009	CaAl ₂ Si ₄ O ₁₀ (OH) ₂											
Pyrite	5.05	0.02	0.01	0.1		Fe ₂ S											
Talc	2.75			0.1	0.01 ^d	Mg ₃ Si ₄ O ₁₀ (OH) ₂											
TOTAL:		1.17	1.06	0.83	0.47												

Table 3. Hydrothermal fluxes

	Unit factor (mol/yr)	LAVAS		LAVA-DIKE TZ		SHEETED DIKES		LOWER CRUST		FULL CRUST		Total Flux ^a
		WR	WR + Veins	WR	WR + Veins	WR	WR + Veins	WR	WR + Veins	WR	WR + Veins	% of Macquarie crustal budget
Si	x10 ¹¹	-8.1 to 3.2	-1.8 to 9.5	0.1 to 1.4	0.2 to 1.5	-0.8 to 6.6	2.5 to 9.9	-22 to -16	-18 to -12	-25 to -10	-12 to 3.3	-0.6 to 0.2
Ti	x10 ¹⁰	-23 to -11	-23 to -11	0.04 to 0.3	0.04 to 0.3	-2.0 to 6.9	-2.1 to 6.9	-5.9 to 1.7	-5.8 to 1.8	-25 to -8.4	-25 to -8.1	-3 to -8
Al	x10 ¹¹	-4.9 to 3.4	-4.3 to 4.1	-1.3 to -0.9	-1.2 to -0.8	-14 to -5.7	-12.9 to -4.6	-8.4 to 8.2	-7.6 to 9.0	-22 to -1.6	-19 to 1.0	-2 to 0.1
Fe	x10 ¹¹	-11 to -4.5	-9.5 to -2.9	-0.1 to 0.2	-0.1 to 0.2	-1.4 to 3.2	0.3 to 5.0	2.3 to 7.2	2.9 to 7.8	-7.0 to 2.5	-2.8 to 6.6	-1 to 3
Mn	x10 ⁹	-7.9 to 4.3	-7.5 to 4.7	0.3 to 0.9	0.3 to 0.9	-2.7 to 9.7	-1.7 to 10	-5.8 to 3.8	-5.2 to 4.3	-8.5 to 11	-6.6 to 13	-2 to 3
Mg	x10 ¹¹	8.2 to 18	10 to 20	-0.5 to -0.1	-0.4 to 0	-2.5 to 3.3	-1.1 to 4.8	6.7 to 24	7.7 to 25	18 to 39	23 to 44	5 to 10
Ca	x10 ¹²	-1.6 to -0.9	-1.6 to -0.9	-0.2 to -0.1	-0.2 to -0.1	-2.2 to -1.6	-2.2 to -1.6	-2.1 to -1.2	-2.0 to -1.1	-5.6 to -4.3	-5.5 to -4.2	-8 to -10
Na	x10 ¹¹	-1.2 to 6.4	-1.2 to 6.3	0.7 to 1.0	0.7 to 1.0	7.4 to 12	7.3 to 12	7.1 to 12	7.3 to 13	18 to 28	18 to 28	8 to 13
K	x10 ¹⁰	21 to 34	23 to 35	1.8 to 2.8	1.8 to 2.8	4.1 to 12	4.1 to 12	-2.4 to 8.6	-2.3 to 8.7	32 to 50	36 to 52	27 to 42
S	x10 ¹⁰	-3.5 to -7.4	-3.2 to 0.7	1.9 to 4.8	1.9 to 4.8	-3.3 to 2.0	14 to 20	1.8 to 5.1	1.7 to 5.1	-3.3 to 4.7	19 to 27	76 to 108
H₂O	x10 ¹²	4.6 to 5.9	4.9 to 6.2	0.23 to 0.31	0.24 to 0.32	4.0 to 4.9	4.3 to 5.2	7.3 to 8.8	7.4 to 8.9	17 to 19	18 to 20	195 to 220
Cu	x10 ⁸	-16 to -4.0		-1.3 to -0.4		-46 to -26		-25 to -11		-78 to -51		-25 to -38
Zn	x10 ⁸	-4.3 to 2.8		0.4 to 0.8		-9.4 to -2.9		-2.8 to 2.5		-12 to -1.0		-1 to -9
Rb	x10 ⁸	0.9 to 3.6		0.2 to 0.3		-0.6 to 0.4		-2.8 to -1.0		-1.2 to 2.2		-8 to 15
Sr	x10 ⁸	-22 to -4.5		-0.9 to 0.1		-5.5 to 7.5		11 to 30		-7.1 to 22		-2 to 5
Cs	x10 ⁶	2.0 to 5.9		-0.01 to 0.05		-0.8 to -0.2		-2.4 to -1.2		-0.5 to 3.7		-5 to 42
Ba	x10 ⁸	6.4 to 18		1.0 to 2.0		-0.5 to 8.7		-10 to -0.2		3.8 to 22		3 to 17
U	x10 ⁶	-0.3 to 1.1		0.02 to 0.05		-1.6 to -0.7		-1.8 to -0.7		-3.0 to -1.0		-12 to -4

Table 4. Comparison of Estimated Hydrothermal Chemical Changes and Fluxes

Average Bulk Crustal Chemical Changes (Δm_i):			Extrapolated Global Hydrothermal Element Fluxes:				
gains (+) and losses (-)			(+ve, net flux to crust; -ve net flux to the oceans)				
ODP ^a		MQ ^b	ODP ^c		MQ ^d	Axial Fluids ^e	Flank Fluids ^e
MAJOR ELEMENTS							
	<i>g/100g</i>	<i>g/100g</i>		<i>10¹² mol/yr</i>	<i>10¹² mol/yr</i>	<i>10¹² mol/yr</i>	<i>10¹² mol/yr</i>
SiO ₂	0.237	-0.30 to 0.08	Si	2.78	-1.17 to 0.33	-0.66 to -0.43	-1.8 to -1.3
TiO ₂	[0] ^f	-0.08 to -0.03	Ti	[0] ^f	-0.25 to -0.08	-	-
Al ₂ O ₃	-	-0.42 to 0.02	Al	1.89	-1.94 to 0.10	-0.0006 to -0.0001	-
FeO _T	-	-0.09 to 0.20	Fe	-	-0.28 to 0.66	-0.19 to -0.02	-
MnO	-	-0.002 to 0.004	Mn	-	-0.01 to 0.01	-0.034 to -0.011	-
MgO	-0.157	0.39 to 0.75	Mg	-2.75	2.26 to 4.35	1.6	0.7 to 1.1
CaO	0.134	-1.3 to -1.0	Ca	1.68	-5.48 to -4.16	-1.3 to -0.009	-0.55 to -0.20
Na ₂ O	0.0655	0.24 to 0.37	Na	1.49	1.79 to 2.81	-	-
K ₂ O	0.0485	0.07 to 0.1	K	0.36	0.33 to 0.52	-0.69 to -0.23	0.1 to 0.64
H ₂ O	0.449	1.35 to 1.52	H ₂ O	17.6	17.6 to 19.8	-	-
S	-0.004	0.03 to 0.04	S	-0.08	0.19 to 0.27	-0.12 to 0.76	-8.0
TRACE ELEMENTS							
	<i>mg/kg</i>	<i>mg/kg</i>		<i>10⁸ mol/yr</i>	<i>10⁸ mol/yr</i>	<i>10⁸ mol/yr</i>	<i>10⁸ mol/yr</i>
Cu	-	-21 to -14		-	-78 to -51	-13 to -3	-
Zn	-	-3.3 to -0.3		-	-12 to -1.0	-32 to -12	-
Rb	0.927	-0.4 to 0.8		0.77	-1.2 to 2.2	-9.5 to -2.6	1.9 to 2.8
Cs	0.0172	-0.003 to 0.02		0.01	-0.005 to 0.04	-0.06 to -0.03	0.020 to 0.023
Sr	1.4	-2.6 to 8.3		11	-7.1 to 22	0	-
Ba	-	2.2 to 13		-	3.8 to 22	-13 to -2.4	2
U	0.0375	-0.03 to -0.01		0.11	-0.03 to -0.01	-	0.1

Supplementary Material for ‘Hydrothermal contributions to global biogeochemical cycles; insights from the Macquarie Island ophiolite’.

Rosalind M. Coggon, Damon A.H. Teagle, Michelle Harris, Garry J. Davidson, Jeffrey C. Alt, and Timothy S. Brewer.

1. Uncertainties

1.1 Uncertainties in Calculated Chemical Changes (Δm_i)

The methods for calculating precursor compositions are subject to the following errors:

(i) analytical errors, (ii) the errors that result from any unaccounted for net changes in mass; and (iii) the errors in calculated precursor-mobile element concentrations due to the broad range of fresh sample compositions at a given immobile monitor element concentration, which we term the primary magmatic error. The errors in estimating precursor compositions and elemental mass changes Δm_i are propagated on a sample-by-sample basis, as follows:

$$\delta(\Delta m_i) = \sqrt{\left(M^o \frac{c_x^o}{c_x^A} c_i^A\right)^2 \left[\left(\frac{\delta(c_x^o/c_x^A)}{(c_x^o/c_x^A)}\right)^2 + \left(\frac{\delta c_i^A}{c_i^A}\right)^2 \right] + (M^o \delta c_i^o)^2}$$

where: $\delta(\Delta m_i X)$ is the error in the calculated elemental mass change; M^o is the total mass of the precursor, c_i^A and c_i^o are the concentrations of component i in the altered rock and the precursor, respectively; c_x^A and c_x^o are the concentrations of an immobile element in the altered rock and the precursor, respectively; $\delta(c_x^o/c_x^A)$ is the error in the ratio of the concentration of the immobile monitor element in the precursor and altered rock due to any unaccounted for net changes in mass; δc_i^A is the analytical

uncertainty in the measured concentration of component i , and δc_i^0 is the primary magmatic error.

The accuracy and precision of major and trace element analyses are provided in Tables S3, S4 and S5. For the purposes of error propagation we assume that the analytical uncertainty in c_i^A is 5% for major elements and 10% for sulfur and trace elements. Given the evidence that net mass changes were typically <5% we assume that $(c_x^0/c_x^A) = 1 \pm 0.05$.

The primary magmatic error in the precursor concentration of an element determined from its magmatic trend with an immobile monitor element (Zr on Nb) is given by:

$$\delta c_i^0 = \sqrt{(STEc_i^0)^2 + (A\delta c_x^0)^2}$$

where $STEc_i^0$ is the standard error of the estimate from the regression (i.e one standard deviation of the residuals of fresh rock concentrations from the regression line, presented in Table S5), A is the slope of the regression line and δc_x^0 is the analytical uncertainty in the immobile monitor element concentration (10%). Precursor-concentrations of elements that show no significant correlation with immobile monitor element concentrations are calculated as the mean concentration of the fresh and/or least altered samples, and the primary magmatic error is taken as one standard deviation of the mean (Table S6). Where altered rocks are compared to a single least-altered sample a primary magmatic error of $\pm 10\%$ is assumed.

1.2 Uncertainties in Average Hydrothermal Fluxes.

The calculated changes in composition of the Macquarie crust due to hydrothermal alteration are converted into net fluxes to or from the crust, using the equation:

$$F_i = \sum_t^T \Delta \bar{m}_{i-t} z_t \rho_c$$

Where: F_i is the mass flux of component i through 1 m^2 of seafloor due to alteration of a section of crust of thickness T ; $\Delta \bar{m}_{i-t}$ is the mean change in mass of component i per unit mass of rock in each sub-interval t ; z_t is the thickness of each sub-interval t ; and ρ_c is the density of the crust (2900 kg/m^3). The uncertainty in the net flux (δF_i) is propagated from the standard error of the mean chemical change of each sub-interval ($\delta \Delta \bar{m}_{i-t}$) as follows:

$$\delta(F_i) = \sqrt{\sum_t^T [(\delta \Delta \bar{m}_{i-t}) z_t]^2}$$

References:

- Jochum, K.P., Nohl, U., Herwig, K., Lammel, E., Stoll, B., Hofmann, A.W., 2005. GeoReM: A New Geochemical Database for Reference Materials and Isotopic Standards. *Geostandards and Geoanalytical Research* 29, 333-338.
- Kamenetsky, V.S., Everard, J.L., Crawford, A.J., Varne, R., Eggins, S.M., Lanyon, R., 2000. Enriched end-member of primitive MORB melts: petrology and geochemistry of glasses from Macquarie Island (SW Pacific). *Journal of Petrology* 41, 411-430.
- Norrish, K., Hutton, J.T., 1969. An accurate X-ray spectrographic method for the analysis of a wide range of geological samples. *Geochimica et Cosmochimica Acta* 33, 431-453.

Wertz, K.L., 2003. From seafloor spreading to uplift: the structural and geochemical evolution of Macquarie Island on the Australian-Pacific plate boundary. University of Texas, Austin, p. 169.

Table S1. Summary of the primary mineralogy and textures and the metamorphism of the igneous lithologies on Macquarie Island.

LITHOLOGY	TEXTURES	PRIMARY MINERALOGY	SECONDARY MINERALOGY		ALTERATION INTENSITY
			PRIMARY MINERAL REPLACEMENT	VEINS	
BASALT LAVAS Pillow lavas, massive basalt, hyaloclastite breccia and feeder dikes	Glassy to fine-grained; sub-ophitic to intersertal; aphyric to highly phyrlic	Phenocrysts: <ul style="list-style-type: none"> Plagioclase: <25-30 vol%; on average 1-3 mm (up to 30 mm) Olivine: < 3 vol%, 1-3 mm Clinopyroxene: <2 vol%, 1-3 mm Spinel (reddish-brown): < 1 vol% 	OFW: <ul style="list-style-type: none"> Olivine: calcite + smectite Interstitial glass: smectite + phillipsite + calcite ZF: <ul style="list-style-type: none"> Olivine: smectite + calcite ± chlorite Plagioclase: zeolite ± sericite ± k-feldspar Interstitial glass: smectite + calcite ± chlorite LGF: <ul style="list-style-type: none"> Olivine: chlorite Plagioclase: albite ± sericite ± chlorite ± prehnite ± epidote ± titanite Spinel: titanite 	OFW: calcite, smectite, celadonite, phillipsite, saponite, hematite, iron-oxyhydroxides Amygdales filled with: smectite + calcite ZF: Na, K, Ca zeolites ± smectite ± calcite ± chlorite ± albite Amygdales filled with: smectite + calcite LGF: Chlorite ± albite ± k-feldspar ± prehnite ± epidote Amygdales filled with: albite ± k-feldspar ± prehnite	Alteration pervasive, extent highly variable (primarily controlled by abundance of olivine and glass)
DOLERITE DIKES	Crypto-crystalline to fine-grained; sub-ophitic to intergranular, aphyric to highly phyrlic	Groundmass: plagioclase + clinopyroxene ± olivine + oxides Phenocrysts: <ul style="list-style-type: none"> Plagioclase: typically <35 vol% (up to 85 vol%); 0.5-15 mm Olivine: ~2.5 vol% (up to 10 vol%); 0.2-4 mm (up to 10 mm) Clinopyroxene: ~ 2 vol% (up to 9 vol%); 0.5-5 mm Spinel (reddish-brown): < 1 vol%; 0.1-0.6 mm 	LGF: <ul style="list-style-type: none"> Plagioclase: plagioclase ± sericite ± prehnite ± epidote ± titanite ± chlorite/smectite Olivine: chlorite ± smectite ± calcite ± sulphides Clinopyroxene and spinel: relatively fresh UGF/LAF: <ul style="list-style-type: none"> Plagioclase: as in LGF dikes Olivine: smectite/chlorite ± sulphides; tremolite + chlorite ± talc ± magnetite Clinopyroxene: (uralitised); actinolite ± tremolite ± hornblende 	LGF: Epidote, CaCO ₃ , chlorite, smectite, secondary plagioclase, pyrite, quartz, zeolite, prehnite UGF/LAF: amphibole, epidote, CaCO ₃ , chlorite, smectite, secondary plagioclase, pyrite, quartz, zeolite, prehnite	Moderately to highly altered: greatest in the upper greenschist/lower amphibolite facies dikes

LITHOLOGY	TEXTURES	PRIMARY MINERALOGY	SECONDARY MINERALOGY		ALTERATION INTENSITY
			PRIMARY MINERAL REPLACEMENT	VEINS	
GABBROS Gabbro, anorthosite and olivine gabbro	Fine-grained porphyritic; medium-grained to pegmatitic hypidiomorphic granular to poikilitic	<ul style="list-style-type: none"> Plagioclase: anhedral to subhedral, tabular to equant; euhedral to sub-rounded chadacrysts Clinopyroxene: medium-grained anhedral ; coarse-grained to pegmatitic anhedral to subhedral poikilitic Olivine: anhedral; sub-rounded chadacrysts 	<ul style="list-style-type: none"> Plagioclase: secondary plagioclase ± prehnite ± epidote ± CaCO₃ ± clay Clinopyroxene: amphibole ± chlorite ± clay ± CaCO₃ ± magnetite Olivine: amphibole ± chlorite ± talc ± sulphides ± serpentine ± magnetite ± clay 	<p>Gabbro and olivine gabbro: amphibole, chlorite, epidote, clinozoisite, zoisite, secondary plagioclase, prehnite, quartz</p> <p>Anorthosite: secondary plagioclase, chlorite, amphibole, epidote, clinozoisite, prehnite, CaCO₃, quartz</p>	Highly variable; slightly to highly altered under greenschist to amphibolite facies conditions
Troctolite, olivine gabbro, wehlite, plagioclase dunite and dunite	Medium-grained to pegmatitic; ad- to ortho-cumulates	<ul style="list-style-type: none"> Olivine: anhedral to euhedral; cumulus phase Clinopyroxene: subhedral to anhedral; post cumulus phase Plagioclase: subhedral to anhedral; cumulus and/or post cumulus phase Spinel: < 1 vol%, dark brown 	<ul style="list-style-type: none"> Olivine: serpentine + magnetite; or amphibole ± chlorite ± talc ± sulphides ± serpentine ± magnetite ± clay Clinopyroxene: amphibole ± chlorite ± clay ± magnetite Plagioclase: prehnite + chlorite + serpentine + secondary plagioclase 	Serpentine ± magnetite, chlorite, talc, prehnite, CaCO ₃	Highly to completely altered; serpentinised
HARZBURGITE	Medium- to coarse-grained Cumulates?	<ul style="list-style-type: none"> Olivine: anhedral; cumulus phase? Orthopyroxene: irregular, <40 vol% Spinel: ~2 vol%, dark brown, irregular 	<ul style="list-style-type: none"> Olivine: serpentine + magnetite; talc, clay, amphibole Orthopyroxene: serpentine + talc (bastite); amphibole 	Serpentine ± magnetite, chlorite, talc, prehnite, CaCO ₃	Highly to completely altered; serpentinised

OFW = ocean floor weathering; ZF = zeolite facies; LGF = lower greenschist facies; UGF = upper greenschist facies; LAF = lower amphibolite facies.

Table S2. Macquarie Island whole rock geochemistry

- see excel sheet.

Table S3. Accuracy and precision for XRF major and trace elements analyses at the University of Leicester.

Standard	NIM-G [n=4]				W-1 [n=3]				BCS372/1 [n=4]			
	Mean Value	Preferred Value	Precision (% RSD)	Accuracy (% RMSD)	Mean Value	Preferred Value	Precision (% RSD)	Accuracy (% RMSD)	Mean Value	Preferred Value	Precision (% RSD)	Accuracy (% RMSD)
SiO₂	75.87	75.70	0.41	0.32	52.36	52.46	0.06	0.10	20.23	20.50	0.34	0.28
TiO₂	0.10	0.09	12	0.01	1.01	1.07	6.5	0.08	0.16	0.16	8.4	0.01
Al₂O₃	11.95	12.08	0.44	0.14	15.04	15.00	0.60	0.08	5.03	3.77	2.3	1.3
Fe₂O₃	2.06	2.02	5.0	0.10	11.13	11.11	0.77	0.07	3.35	4.82	1.5	1.5
MnO	0.02	0.02	11	0.00	0.17	0.17	1.6	0.00	0.06	0.06	9.0	0.01
MgO	0.02	0.06	299	0.07	6.60	6.62	3.0	0.16	1.48	2.42	9.8	0.95
CaO	0.75	0.78	5.7	0.05	10.93	11.00	1.3	0.14	64.75	64.80	0.45	0.26
Na₂O	3.49	3.36	2.9	0.16	2.23	2.16	3.8	0.10	0.27	0.10	10	0.17
K₂O	5.01	4.99	0.91	0.04	0.63	0.64	4.9	0.03	0.73	0.49	0.94	0.24
P₂O₅	0.01	0.01	13	0.00	0.13	0.13	1.3	0.00	0.08	0.08	3.1	0.004
Total	99.63	99.11	0.28	0.57	100.18	100.36	0.33	0.33	96.72	97.14	0.45	0.57

Standard	BIR-1 [n=7]				BCR-1 [n=7]				JR-1 [n=7]			
	Mean Value	Preferred Value	Precision (% RSD)	Accuracy (% RMSD)	Mean Value	Preferred Value	Precision (% RSD)	Accuracy (% RMSD)	Mean Value	Preferred Value	Precision (% RSD)	Accuracy (% RMSD)
Cr	394	382	2.7	16	19	16	23	5.4	7.8	2	57	7.1
Cu	126	126	1.9	2.3	28	19	12	9.9	0.40	1	75	0.7
Ni	166	166	2.2	3.4	13	13	13	1.5	2.6	1	56	2.1
Sc	41	44	4.8	3.7	33	33	3.9	1.2	4.0	5	19	1.2
V	301	313	8.2	26	395	407	1.4	13	8.5	-	40	-
Zn	70	71	1.1	0.90	128	130	0.90	2.0	30.1	30	3.0	0.8
Zr	17	22	29	6.8	193	190	1.1	3.2	99.0	102	5.7	6.0

Accuracy is reported as the relative root-mean square deviation (%RMSD) compared to the preferred reference value.

Table S4. Accuracy, precision and limits of detection for trace elements analyzed by ICP-MS at the University of Southampton.

	JB-1a [n=8]				JA-1 [n=6]				BHVO-1 [n=3]				Average precision (%RSD)	Average accuracy (%RMSD)
	Mean Value	Preferred Value ¹	Precision (%RSD)	Accuracy (%RMSD)	Mean Value	Preferred Value ¹	Precision (%RSD)	Accuracy (%RMSD)	Mean Value	Preferred Value ¹	Precision (%RSD)	Accuracy (%RMSD)		
Rb	40.9	39	0.8	5.1	11.5	10.65	8.9	11.8	9.76	9.19	9.3	10.2	6.3	9.0
Sr	444	444	1.9	1.8	254	264	3.3	4.7	391	396	1.3	1.7	2.2	2.7
Y	23.9	24	3.8	3.6	30.0	29	3.1	4.5	27.3	26	1.3	5.1	2.7	4.4
Zr	145	142	1.3	2.5	89.0	84	3.1	6.6	179	174	1.3	2.8	1.9	4.0
Nb	27.2	28	1.7	3.3	1.47	1.4	18.4	18.4	18.1	18.6	4.8	4.7	8.3	8.8
Cs	1.31	1.2	4.4	10.0	0.64	0.64	5.1	4.7	0.11	0.101	4.1	12.4	4.5	9.0
Ba	509	489	2.0	4.6	297	303	3.4	3.6	128	133	1.8	3.7	2.4	4.0
La	36.8	38	1.3	3.4	4.6	5	2.7	8.6	14.7	15.5	2.5	5.2	2.2	5.7
Ce	68.4	66	6.7	7.5	13.0	13.5	2.5	4.4	38.0	38.1	1.0	0.9	3.4	4.3
Pr	6.76	7.2	3.3	6.8	1.98	2.08	1.8	5.0	5.08	5.42	1.5	6.3	2.2	6.0
Nd	25.8	26.3	3.5	3.8	10.5	10.9	1.3	4.2	24.6	24.7	2.9	2.3	2.6	3.4
Sm	4.96	5.10	4.4	4.8	3.27	3.4	2.4	4.5	6.02	6.12	1.6	2.0	2.8	3.8
Eu	1.45	1.46	3.6	3.5	1.08	1.12	1.1	3.5	2.06	2.09	1.7	2.1	2.1	3.0
Gd	4.71	4.70	12.8	12.0	4.01	4.20	2.1	5.0	6.00	6.33	2.5	5.6	5.8	7.5
Tb	0.69	0.72	7.8	8.3	0.71	0.73	1.6	3.4	0.92	0.96	2.9	4.3	4.1	5.3
Dy	4.02	4.10	4.5	4.6	4.66	4.80	1.5	3.3	5.22	5.31	2.3	2.4	2.8	3.4
Ho	0.82	0.83	5.1	4.9	1.01	1.05	1.6	3.8	0.97	0.98	2.6	2.2	3.1	3.7
Er	2.22	2.20	5.2	5.0	2.92	3.00	1.1	3.0	2.47	2.55	1.0	3.4	2.4	3.8
Tm	0.30	0.30	4.3	4.1	0.44	0.44	8.7	7.9	0.31	0.33	2.4	6.1	5.2	6.1
Yb	2.02	2.16	3.9	7.4	2.86	3.00	1.9	4.9	1.92	2.00	0.7	4.3	2.2	5.5
Lu	0.31	0.31	5.5	5.3	0.47	0.45	4.0	5.2	0.28	0.27	1.3	5.4	3.6	5.3
Hf	3.40	3.50	6.1	6.2	2.45	2.50	1.6	2.4	4.09	4.46	2.2	8.5	3.3	5.7
Pb	7.16	6.30	4.3	14.4	6.43	5.80	1.6	10.9	2.51	2.40	11.9	11.1	5.9	12.1
Th	8.83	9.20	0.7	4.1	0.77	0.76	5.8	5.3	1.25	1.23	2.2	2.4	2.9	3.9
U	1.52	1.60	9.4	9.7	0.32	0.35	6.9	10.5	0.38	0.41	5.2	8.7	7.1	9.6

1: preferred reference values from GeoReM (Jochum et al., 2005). Accuracy is reported as the relative root-mean square deviation (%RMSD) compared to the preferred reference value. A synthetic calibration was used for Ta.

Table S5. Precursor compositions of whole rock samples from fractionated melts

	LAVAS AND DIABASE DIKES	GABBRO	ANORTHOSITE
Major elements (Wt %)			
SiO ₂	49.5 ± 0.7 [n = 96]		46.2 ± 0.4 [n = 2]
TiO ₂	0.007 (Zr) + 0.7 ± 0.1 [R ² = 0.78; n = 92]	0.19 ± 0.04 [n = 5]	0.05 ± 0.01 [n = 2]
Al ₂ O ₃	16.8 ± 0.7 [n = 98]	18.7 ± 2.9 [n = 5]	31.5 ± 0.8 [n = 2]
FeO _T	8.98 – 0.028 (Nb) ± 0.52 [R ² = 0.41; n = 93]	3.52 ± 0.74 [n = 5]	1.02 ± 0.45 [n = 2]
MnO	0.17 – 0.0008 (Nb) ± 0.02 [R ² = 0.22; n = 93]	0.08 ± 0.02 [n = 5]	0.01 ± 0.01 [n = 2]
MgO	9.42 – 0.018 (Zr) ± 0.48 [R ² = 0.59; n = 97]		1.5 ± 0.8 [n = 2]
CaO	15.7 – 0.037 (Zr) ± 0.55 [R ² = 0.84; n = 99]		
Na ₂ O	0.012 (Zr) + 1.79 ± 0.33 [R ² = 0.59; n = 97]		2.4 ± 0.4 [n = 2]
K ₂ O	0.018 (Nb) + 0.023 ± 0.09 [R ² = 0.93; n = 99]		
P ₂ O ₅	0.006 (Nb) + 0.085 ± 0.04 [R ² = 0.83; n = 93]	0.003 ± 0.001 [n = 5]	0.003 ± 0.005 [n = 2]
H ₂ O	0.015 (Nb) + 0.18 ± 0.10 [R ² = 0.85; n = 89] ^a		
S	0.08 ± 0.01 [n = 98]	0.03 ± 0.01 [n = 5]	0.01 ± 0.007 [n = 2]
Trace elements (ppm)			
Cu	183 – 0.8 (Zr) ± 10 [R ² = 0.58; n = 33] ^a	40 ± 24 [n = 5]	56
Zn	56 ± 10 [n = 37]	13 ± 5 [n = 5]	11
Rb	0.68 (Nb) – 3.1 ± 1.6 [R ² = 0.98; n = 89] ^a	0.87 ± 0.55 [n = 5]	2.3 ± 1.8 [n = 2]
Sr	5.7 (Nb) + 100 ± 38 [R ² = 0.87; n = 99]		
Cs	0.008 (Nb) – 0.067 ± 0.03 [R ² = 0.95; n = 59]	0.01 ± 0.005 [n = 4]	0.008 ± 0.001 [n = 2]
Ba	6.5 (Nb) – 20 ± 19 [R ² = 0.97; n = 93]	16 ± 10 [n = 5]	18 ± 12 [n = 2]
La	0.505 (Nb) + 1.38 ± 1.1 [R ² = 0.98; n = 99]		
Lu	0.38 ± 0.06 [n = 93]	0.08 ± 0.03 [n = 5]	0.009 ± 0.005 [n = 2]
U	0.022 (Nb) – 0.03 ± 0.08 [R ² = 0.95; n = 93]	0.011 ± 0.010 [n = 4]	0.004 ± 0.003 [n = 2]

Precursor compositions determined from analyses of Macquarie glasses (Kamenetsky et al., 2000; Wertz, 2003), supplemented with analyses of the least altered whole rock samples, including: aphyric dike chilled margins (MQ 47A and 105B); aphyric dikes (MQ 61 and 69A); gabbros (MQ 40, 45A, 85, 87 and 115A); and anorthosites (MQ 59 and 92). ^a Glass samples only used to determine precursor trend. Major elements: wt%; trace elements (including Zr and Nb): ppm. R² = regression coefficient; n = number of

fresh precursor samples that the regression line or average composition was determined from. Primary magmatic errors (red type) were calculated as one standard deviation of the residuals of precursor compositions from regression lines, or one standard deviation of precursor compositions for elements that show no trend with Nb or Zr. For some elements magmatic trends could not be extended to anorthosite \pm gabbro compositions; for these elements average values of least-altered samples are used. Fe is recalculated to total FeO ($\text{FeO}_T = 0.8998 \text{ Fe}_2\text{O}_{3T}$) to allow comparison with analyzed glass Fe concentrations.

Table S6. Precursor compositions of porphyritic lavas and dikes, and olivine gabbro samples.

PORPHYRITIC LAVAS AND DIKES:			
	Nb <20 ppm:	Nb > 20 ppm:	OLIVINE GABBRO:
	MAQ 222B	MQ58	MQ 68A
	MQ12	MAQ119	MQ 74B
	MQ98	MAQ 134	MQ 75
	MQ102	MAQ 139B	
	MAQ 126B	MAQ 136, MQ 89	
Major elements (Wt %)			
SiO ₂	49.2 ± 0.7	49.7 ± 1.1	49.5 ± 1.3
TiO ₂	1.05 ± 0.22	1.80 ± 0.36	0.17 ± 0.08
Al ₂ O ₃	17.4 ± 2.4	16.2 ± 1.8	16.4 ± 2.9
FeO _T	7.70 ± 1.26	9.16 ± 1.5	3.61 ± 0.38
MnO	0.13 ± 0.03	0.15 ± 0.02	0.08 ± 0.01
MgO	7.83 ± 1.31	6.18 ± 0.71	10.5 ± 0.4
CaO	12.2 ± 0.6	10.42 ± 0.99	16.87 ± 1.81
Na ₂ O	2.93 ± 0.17	4.08 ± 0.55	1.52 ± 0.12
K ₂ O	0.16 ± 0.09	0.38 ± 0.19	0.08 ± 0.02
P ₂ O ₅	0.12 ± 0.05	0.33 ± 0.05	0.002 ± 0.002
S	0.008 ± 0.006	0.005 ± 0.003	0.02 ± 0.02
H ₂ O	1.27 ± 0.48	1.60 ± 0.31	1.22 ± 0.13
Trace elements (ppm)			
Cu	19.0 ± 19.5	32.1 ± 25.9	39.9 ± 32.5
Zn	27.9 ± 14.4	55.4 ± 2.1	13.4 ± 4.1
Rb	2.66 ± 3.14	6.56 ± 5.49	0.45 ± 0.18
Sr	182 ± 38	230 ± 54	92.6 ± 10.0
Cs	0.021 ± 0.031	0.055 ± 0.051	0.015 ± 0.013
Ba	49.4 ± 41.5	131 ± 31	6.57 ± 4.29
La	5.03 ± 2.72	17.8 ± 1.0	0.26 ± 0.05
Lu	0.28 ± 0.11	0.45 ± 0.13	0.09 ± 0.04
U	0.143 ± 0.138	0.46 ± 0.13	0.004 ± 0.001

Table S7. Hydrothermal fluxes (kg/m²)

	Unit factor	LAVAS		LAVA-DIKE TZ		SHEETED DIKES		LOWER CRUST		UPPER CRUST		FULL CRUST	
		WR	WR + Veins	WR	WR + Veins	WR	WR + Veins	WR	WR + Veins	WR	WR + Veins	WR	WR + Veins
SiO ₂	x10 ⁴	-1.6 to 0.6	-0.4 to 1.9	0.02 to 0.27	0.04 to 0.30	-0.2 to 1.3	0.5 to 2.0	-3.1 to -4.4	-2.4 to -3.7	-1.1 to 1.6	0.8 to 3.5	-2.0 to -5.0	-2.3 to 0.7
TiO ₂	x10 ³	-3.0 to -6.2	-2.9 to -6.2	0.01 to 0.08	0.01 to 0.08	-0.5 to 1.8	-0.5 to 1.8	-1.6 to 0.4	-1.6 to 0.5	-1.9 to -5.9	-1.9 to -5.9	-2.2 to -6.7	-2.2 to -6.6
Al ₂ O ₃	x10 ³	-8.4 to 5.8	-7.3 to 6.9	-1.5 to -2.2	-1.4 to -2.1	-9.7 to -24	-7.8 to -22	-14 to 14	-13 to 15	-10 to -30	-6.8 to -27	-2.8 to -37	-33 to 1.7
FeO	x10 ³	-11 to -27	-6.8 to -23	-0.23 to 0.39	-0.12 to 0.50	-3.5 to 7.7	0.7 to 12	5.4 to 17	7.0 to 19	-6.9 to -26	-18 to 1.4	-17 to 6	-6.8 to 16
MnO	x10 ²	-1.9 to 1.0	-1.8 to 1.1	0.07 to 0.22	-0.20 to -0.31	-0.6 to 2.3	-0.4 to 2.5	-1.4 to 0.9	-1.2 to 1.0	-1.5 to 2.6	-1.2 to 3.0	-2.0 to 2.7	-1.6 to 3.1
MgO	x10 ⁴	1.1 to 2.4	1.3 to 2.7	-0.01 to -0.07	-0.06 to 0	-0.3 to 0.4	-0.1 to 0.6	0.9 to 3.2	1.0 to 3.4	1.0 to 2.6	1.5 to 3.0	2.5 to 5.3	3.0 to 5.9
CaO	x10 ⁴	-1.7 to -3.0	-1.6 to -3.0	-0.20 to -0.31	-0.20 to -0.31	-3.0 to -4.1	-3.0 to -4.1	-2.2 to -3.9	-2.1 to -3.8	-5.3 to -7.1	-5.2 to -6.9	-8.0 to -10	-7.8 to -10
Na ₂ O	x10 ³	-1.2 to 6.6	-1.2 to 6.6	0.71 to 1.1	0.70 to 1.1	7.7 to 12	7.6 to 12	7.3 to 13	7.6 to 13	9.0 to 18	8.9 to 18	18 to 29	18 to 29
K ₂ O	x10 ³	3.4 to 5.3	3.6 to 5.5	0.28 to 0.44	0.27 to 0.44	0.65 to 1.9	0.64 to 1.9	-0.38 to 1.4	-0.36 to 1.4	4.8 to 7.1	5.0 to 7.4	5.0 to 7.9	5.3 to 8.2
S	x10 ²	-3.7 to -7.9	-3.4 to 0.8	2.0 to 5.1	2.0 to 5.2	-3.5 to 2.2	15 to 21	1.9 to 5.5	1.9 to 5.5	-6.8 to 0.9	17 to 24	-3.5 to 5.0	20 to 28
LOI	x10 ⁴	2.7 to 3.5	3.0 to 3.7	0.14 to 0.18	0.14 to 0.19	2.4 to 3.0	2.6 to 3.1	4.4 to 5.3	4.4 to 5.4	5.5 to 6.5	5.9 to 6.8	10 to 11	11 to 12
Cu		-8.4 to -33		-1.0 to -2.7		-56 to -98		-23 to -52		-75 to -124		-109 to -165	
Zn		-9.5 to 6.2		0.89 to 1.7		-6.4 to -21		-6.0 to 5.5		-3.3 to -24		-2.1 to -26	
Rb		2.6 to 10		0.55 to 0.94		-1.9 to 1.2		-2.7 to -7.9		2.7 to 11		-3.3 to 6.4	
Sr		-13 to -65		-2.5 to 0.35		-16 to 22		31 to 88		-5.2 to -70		-21 to 65	
Cs		0.09 to 0.26		0 to 0.002		-0.01 to -0.04		-0.05 to -0.11		0.06 to 0.24		-0.02 to 0.17	
Ba		29 to 82		4.7 to 9.3		-2.4 to 40		-1.0 to -46		48 to 116		18 to 99	
U		-0.02 to 0.09		0.001 to 0.004		-0.06 to -0.13		-0.06 to -0.15		-0.12 to 0.01		-0.08 to -0.24	